МІНІСТЕРСТВО ОСВІТИ ТА НАУКИ УКРАЇНИ
Національний авіаційний університет
Кафедра конструкції літальних апаратів

ДОПУСТИТИ ДО ЗАХИСТУ
Завідувач кафедри, к.т.н., доцент
________ Святослав ЮЦКЕВИЧ
«___» ____________ 2024 р.

КВАЛІФІКАЦІЙНА РОБОТА
ЗДОБУВАЧА ОСВІТНЬОГО СТУПЕНЯ
«БАКАЛАВР»

Тема: «Закономірності росту втомних тріщин у конструктивних елементах важкого транспортного літака»

Виконав: __________ **Дмитро СОЛІН**

Керівник: к.т.н., доц. __________ **Володимир КРАСНОПОЛЬСЬКИЙ**

Нормоконтролер: к.т.н., доц. __________ **Володимир КРАСНОПОЛЬСЬКИЙ**

Київ 2024

MINISTRY OF EDUCATION AND SCIENCE OF UKRAINE
National Aviation University
Department of Aircraft Design

PERMISSION TO DEFEND
Head of the department,
Associate Professor, PhD.
_________ Sviatoslav YUTSKEVYCH
"___" ____________ 2024

BACHELOR DEGREE THESIS

Topic: "Fatigue crack growth dependences in structural elements of heavy transport aircraft"

Fulfilled by:	____________	**Dmytro SOLIN**
Supervisor: **PhD, associate professor**	____________	**Volodymyr KRASNOPOLSKYI**
Standards inspector: **PhD, associate professor**	____________	**Volodymyr KRASNOPOLSKYI**

Kyiv 2024

НАЦІОНАЛЬНИЙ АВІАЦІЙНИЙ УНІВЕРСИТЕТ

Аерокосмічний факультет
Кафедра конструкції літальних апаратів
Освітній ступінь «Бакалавр»
Спеціальність 134 «Авіаційна та ракетно-космічна техніка»
Освітньо-професійна програма «Обладнання повітряних суден»

`

ЗАТВЕРДЖУЮ
Завідувач кафедри, к.т.н., доцент
________ Святослав ЮЦКЕВИЧ
«___» ____________ 2024 р

ЗАВДАННЯ

на виконання кваліфікаційної роботи здобувача вищої освіти

СОЛІНА ДМИТРА АНДРІЙОВИЧА

1. Тема роботи: «Закономірності росту втомних тріщин у конструктивних елементах важкого транспортного літака», затверджена наказом ректора від 15 травня 2024 року № 794/ст.
2. Термін виконання роботи: з 20 травня 2024 р. по 16 червня 2024 р.
3. Вихідні дані до роботи: маса комерційного навантаження 200000 кг, дальність польоту з максимальним комерційним навантаженням 4000 км, крейсерська швидкість польоту 860 км/год, висота польоту 9 км.
4. Зміст пояснювальної записки: вступ, основна частина, що включає аналіз літаків-прототипів і короткий опис проектованого літака, обґрунтування вихідних даних для розрахунку, розрахунок основних льотно-технічних та геометричних параметрів літака, компонування пасажирської кабіни, розрахунок центрування літака, спеціальна частина, яка містить аналіз закономірностей росту втомних тріщин у силових конструктивних елементах літака.
5. Перелік обов’язкового графічного (ілюстративного) матеріалу: загальний вигляд літака (А1×1), компонувальне креслення фюзеляжу (А1×1), розрахункові графіки і діаграми.

6. Календарний план-графік:

№	Завдання	Термін виконання	Відмітка про виконання
1	Вибір вихідних даних, аналіз льотно-технічних характеристик літаків-прототипів.	20.05.2024 – 21.05.2024	
2	Вибір та розрахунок параметрів проектованого літака.	22.05.2024 – 23.05.2024	
3	Виконання компонування літака та розрахунок його центрування.	24.05.2024 – 25.05.2024	
4	Розробка креслень по основній частині дипломної роботи.	26.05.2024 – 27.05.2024	
5	Огляд літератури за проблематикою роботи. Проблема втоми авіаційних конструкцій.	28.05.2024 – 29.05.2024	
6	Обробка експериментальних даних. Аналіз закономірностей росту втомних тріщин.	30.05.2024 – 31.05.2024	
7	Оформлення пояснювальної записки та графічної частини роботи.	01.06.2024 – 02.06.2024	
8	Подача роботи для перевірки на плагіат.	03.06.2024 – 06.06.2024	
9	Попередній захист кваліфікаційної роботи.	07.06.2024	
10	Виправлення зауважень. Підготовка супровідних документів та презентації доповіді.	08.06.2024 – 10.06.2024	
11	Захист дипломної роботи.	11.06.2024 – 16.06.2024	

7. Дата видачі завдання: 20 травня 2024 року

Керівник кваліфікаційної роботи ____________ Володимир КРАСНОПОЛЬСЬКИЙ

Завдання прийняв до виконання ____________ Дмитро СОЛІН

NATIONAL AVIATION UNIVERSITY

Aerospace Faculty
Department of Aircraft Design
Educational Degree "Bachelor"
Specialty 134 "Aviation and Aerospace Technologies"
Educational Professional Program "Aircraft Equipment"

APPROVED BY
Head of the department,
Associate Professor, PhD.
_________ Sviatoslav YUTSKEVYCH
"___" ____________ 2024

TASK

for the bachelor degree thesis

Dmytro SOLIN

1. Topic: "Fatigue crack growth dependences in structural elements of heavy transport aircraft", approved by the Rector's order № 794/ст from 15 May 2024.
2. Period of work: since 20 May 2024 till 16 June 2024.
3. Initial data: payload 200 tons, flight range with maximum capacity 4000 km, cruise speed 860 km/h, flight altitude 9 km.
4. Content (list of topics to be developed): introduction, main part: analysis of prototypes and brief description of designing aircraft, selection of initial data, wing geometry calculation and aircraft layout, landing gear design, engine selection, center of gravity calculation, special part: analysis of fatigue cracks growth dependencies of aircraft.
5. Required material: general view of the airplane (A1×1), layout of the airplane (A1×1), schemes, plots and diagrams.

6. Thesis schedule:

№	Task	Time limits	Done
1	Selection of initial data, analysis of flight technical characteristics of prototypes aircrafts.	20.05.2024 – 21.05.2024	
2	Selection and calculation of the aircraft designed parameters.	22.05.2024 – 23.05.2024	
3	Performing of aircraft layout and centering calculation.	24.05.2024 – 25.05.2024	
4	Development of drawings on the thesis main part.	26.05.2024 – 27.05.2024	
5	Analysis of fatigue problem for aviation structures.	28.05.2024 – 29.05.2024	
6	Analysis of experimental data and fatigue crack growth dependences.	30.05.2024 – 31.05.2024	
7	Explanatory note checking, editing, preparation of the diploma work graphic part.	01.06.2024 – 02.06.2024	
8	Submission of the work to plagiarism check.	03.06.2024 – 06.06.2024	
9	Preliminary defense of the thesis.	07.06.2024	
10	Making corrections, preparation of documentation and presentation.	08.06.2024 – 10.06.2024	
11	Defense of the diploma work.	11.06.2024 – 16.06.2024	

7. Date of the task issue: 20 May 2024

Supervisor: ____________ Volodymyr KRASNOPOLSKYI

Student: ____________ Dmytro SOLIN

РЕФЕРАТ

Пояснювальна записка кваліфікаційної роботи бакалавра «Закономірності росту втомних тріщин у конструктивних елементах важкого транспортного літака»:

85 с., 22 рис., 15 табл., 12 джерел

Дана кваліфікаційна робота присвячена розробці вантажного літака для середньомагістральних авіаліній з можливістю транспортування великих/негабаритних вантажів, що відповідає міжнародним стандартам польотів, нормам безпеки, економічності та надійності, а також аналіз закономірностей росту втомних тріщин у навантажених конструктивних елементах крила та фюзеляжу.

В роботі було використано методи аналітичного розрахунку, комп’ютерного проєктування за допомогою CAD/CAM/CAE систем, чисельного моделювання і статистичного аналізу експериментальних даних.

Практичне значення результату кваліфікаційної роботи полягає у виявленні закономірностей росту і розвитку втомних тріщин у традиційних авіаційних алюмінієвих сплавах з метою передбачення та прогнозування граничного стану конструкції.

Матеріали кваліфікаційної роботи можуть бути використані в навчальному процесі та в практичній діяльності конструкторів спеціалізованих проектних установ.

Дипломна робота, аванпроект літака, компонування, центрування, втомна тріщина, закон розподілу

ABSTRACT

Bachelor degree thesis "Fatigue crack growth dependences in structural elements of heavy transport aircraft"

85 pages, 22 figures, 15 tables, 12 references

This thesis is dedicated to design of a cargo airplane for medium haul airlines with the possibility of transporting big/heavy cargo, which meets international flight standards, safety, economy and reliability standards, as well as analysis of the fatigue crack growth dependences in loaded structural elements of the wing and fuselage.

The design methodology is based on prototype analysis to select the most advanced technical decisions, engineering calculations to get the technical data of designed aircraft and computer based design using CAD/CAM/CAE systems. In special part the numerical modeling and statistical analysis is used to process experimental data.

Practical value of the work is to identify the patterns of fatigue cracks growth and development in traditional aviation aluminum alloys in order to predict the limiting state of the structure.

The materials of the qualification work can be used in the aviation industry and educational process of aviation specialties.

Bachelor thesis, preliminary design, cabin layout, center of gravity calculation, fatigue crack, probability distribution law

Format	№	Designation	Name	Quantity	Notes
			<u>General documents</u>		
A4	1	NAU 24 03S 00 00 00 71 TW	Task for work	1	
	2	NAU 24 03S 00 00 00 71	Heavy transport aircraft	2	
A1		Sheet 1	General view	1	
A1		Sheet 2	Fuselage layout	1	
A4	3	NAU 24 03S 00 00 00 71 EN	Heavy transport aircraft	85	
			Explanatory note		

	Sh.	№ doc.	Sign	Date	NAU 24 03S 00 00 00 71 EN		
Done by		Solin D.A..			Fatigue crack growth dependences in structural elements of heavy transport aircraft (List of qualification paper)	list	sheet	sheets
Supervisor		Krasnopolskyi V.S.				Q	9	85
						404 ASF 134		
St.control.		Krasnopolskyi V.S.						
Head of dep.		Yutskevych S.S.						

CONTENT

INTRODUCTION

In the modern day, the cargo aviation market has a lot to offer – from wide-body light transports and up to the giants of the aviation world. However, the latter of those are in quite short supply – one may choose among either converted jumbo jets or a couple of unconventional one-of-a-kind aircraft, such as Airbus Beluga or sorely missed An-225 Mriya, destroyed in the events of war. One may argue that there is no need for such giants anymore, as they may be economically inefficient and may be replaced by larger number of lighter aircraft. While it may be true for conventional ULD cargo (though it is still debatable), it is important to remember that there are a lot of cases of unconventional cargo, too large or too heavy, that those lighter models may only dream of carrying. Moreover, such aircraft may carry large quantities of those goods in one go, which may prove useful for mass manufacturing.

Matter of fact, there is another significant side, interested in such aircraft – the military. The recent events in the world only reinforce the opinion that the world peace is far from achieved and that only strong militaries may provide the necessary means of ensuring the safety of citizens. The military has a lot to transport – and to do it in colossal quantities, such as artillery shells or spare parts for vehicles. Actually, the military would not mind transporting the vehicles themselves. This is the job that only may be provided by the superheavies. The modern MBTs weight between 50-70 tons, and usually are transported by air in quantity of one. It requires a lot of inefficient usage of existing aircraft, or slow transport by other means – and it may be too slow, proven by recent events.

Moreover, there are many players that have a need for transporting an unconventionally large cargo, from aircraft manufacturers to rock bands managers. Often such transports are made by other means, rather slowly and unnecessarily complicated. In case an aircraft is desired – the choice is not large. It may be a converted one with all the drawbacks of restricted access and small cargo compartments; it may be an Antonov model, which are quite hard to get hands on due to their low number and difficult to operate due to outdated electronics and inefficient engines; it may be a special aircraft, which are extremely expensive and hard to get.

Therefore, the task of this project is to make a preliminary design of an aircraft with such goals:

1. To be able to fill the market of ultra-heavy and unconditional transportation.
2. To be able to efficiently carry conventional cargo.
3. To provide military with a way of carrying at least 3 MBTs and other vehicular cargo.
4. To be able to consistently fly on medium-range routes around Europe and America without refueling.
5. To be simple in maintenance.

Therefore, the main performances are taken to be as such: payload of 200000 kg, range of 4000 km, design attitude of 9 km, cruise speed 860 km/h.

There is an important problem that always arises in the operation of an aircraft – the problem of fatigue. This is the process of cumulative damage of aircraft components due to the repeated loading cycles that arise during various flight procedures. As the process has stochastic character, it is required to use statistical methods of analysis on the results of multiple tests to provide safety in operation. It is possible to study the crack growth process in such way to determine the required frequency of maintenance to not allow the crack to grow to critical sizes. Therefore, the special part of the work considers the research of fatigue crack growth dependances in the typical material of the designed aircraft's components.

1. PRELIMINARY DESIGN OF HEAVY AIRCRAFT

1.1 Analysis of prototypes and short description of designed aircraft

The selection of data for the design of aircraft is made based on the market role that it will provide, using the desired performances. On the other hand, it is influenced by the manufacturing and operational factors, such as materials and processing methods, maintenance possibility. The preliminary design of aircraft includes aerodynamic calculations, geometry design and centering of the aircraft, which all will be done in this work.

To understand the general tendencies of the aircraft design on market, it is required to reference some existing competitor aircraft, further referred here as prototypes. For the task of the paper, there are three main aircraft prototypes. They are:

- An-124 "Ruslan" – the largest serial Antonov model, closest to the desired parameters, reliable and robust aircraft, able to use unpaved runways. This aircraft will be the main prototype for the work and the main source of inspiration and reference for the overall shape and characteristics;
- Lockheed C-5 Galaxy – the military transport mainly used by the US Army nowadays. Has lower payload, but greater range and is overall similar to the An-124 in fuselage geometry. For this work it will be the secondary source of data;
- Boeing 747-400F – this aircraft is a converted 747 superjet. As it is not used for exactly same purpose, it may serve as the reference point for the transportational capabilities of the designed aircraft.

The performances of prototypes compared to the designed aircraft are presented in table 1.1.

Table 1.1

Performances of prototypes

Parameter	An-124-100M-150 "Ruslan"	C-5 Galaxy	B747-400F	Designed aircraft
1	2	3	4	5
Max. payload, kg	150000	127500	124330	200000
Crew	4	4-8	2	4-8
Specific wing load, kPa	6.4	6.615	7.338	5.38
Flight range with max. payload, km	3700	4260	7169	4000
Cruise speed, km/h	850	869	933	860
Cruise altitude, km	9	9	11	9
Thrust/weight ratio, N/kg	2.5	2.6	2.85	2.32
Approach speed, km/h	260	250	296	274
Landing speed, km/h	250	240	285	260
Take-off speed, km/h	260	231	342	294
Take-off run distance, m	3000	2500	3300	3496
Landing distance, m	800	1500	2130	1424
Maximum take-off mass, kg	402000	381018	396893	633326
Landing mass, kg	330000	288417	302092	534312
Empty weight, kg	181000	187000	178700	285345
Fuel fraction, %	53	39.6	41	23.4
Payload fraction, %	37.31	33.4	31	31.6
Wing span, m	73.3	68	68.4	96
Sweepback angle at ¼ chord, °	32	25	38	29
Wing aspect ratio	8,6	7.95	7.91	8.60
Wing taper ratio	3.05	2.46	4.07	3.04
Fuselage length, m	69	75.3	70.7	84
Fuselage diameter, m	8.4	7.2	6.2	8.4
Fuselage fineness ratio	8.23	10.46	11.40	10
Horizontal tail span, m	35	21.2	21.4	36
Horizontal tail sweepback angle, °	34	24	37	32
Horizontal tail aspect ratio	5.24	4.87	4	6.51
Horizontal tail taper ratio	2.814	2.48	3.184	2.8
Vertical tail height, m	10.9	10	9.65	16.5
Vertical tail sweepback angle, °	42	34	47	38
Vertical tail aspect ratio	5.35	2.31	2.34	1.35
Vertical tail taper ratio	3.29	1.13	3.34	3.29
Landing gear wheel base, m	23.4	22	24.65	32
Landing gear wheel track, m	8.6	7.9	10.55	8.6

1.2. Short description of aircraft main parts

The aircraft is a cantilever high-wing monoplane with four turbofan engines located on wing and retractable landing gear with a front single-strut landing gear and two main landing gear units. Fuselage has double-bubble cross-section and semi-monocoque design. The design of empennage is conventional.

1.2.1. Wing

The wing is swept, trapezoidal and has geometrical twist, thus providing optimal characteristics for the transonic cruise regimes. In the same considerations, the airfoil is chosen to be supercritical. The wing is anhedral to provide the increased maneuverability for such heavy aircraft with high wing (and keel effect that comes with it).

The wing consists of the center wing and two cantilever outboard parts. It is divided into three sections: wing box that carries all loads, leading and trailing parts.

Six slats' sections are installed on the leading edge of each outboard part. On the trailing edge of each outboard part one inner flap section and two outer flap sections, inner and outer ailerons and nine sections of in-flight spoilers are installed. The flaps are triple-slotted to increase the energy of the upper layer of air. The ailerons are aerodynamically balanced and trimmable via trim tabs. Anti-icing system powered by bleed air ensures the absence of ice on the wing surface.

The wing box in the center section is made of four spars, upper and lower panels and ribs. There are holes in ribs for electronics, inspection and systems pipelines, including the fuel transferring. The wing box in the cantilever parts has four spars, however the middle spars do not extend to all wing length due to the decrease in the wing chord; upper and lower panels and ribs. There are six integral fuel tanks and pipelines between them.

The wing is located in high position, allowing the fuselage to have lower elevation and decreasing the possibility of contamination of engines with dirt from runways.

1.2.2. Fuselage

The fuselage is pressurized, has semi-monocoque design and two decks. The lower deck is cargo bay with reinforced floor that allows carrying of cargo with high mass concentration, such as military vehicles. The upper deck accommodates the cockpit, load masters' quarters and equipment bays. The upper deck is divided into front and rear parts by the wing center section.

In the front and the back of the fuselage large cargo hatches are installed for easy access.

On the upper deck of the fuselage there are two emergency doors and three hatches on the starboard side and one emergency door and one hatch on the port side.

The fuselage also provides various access hatches for inspection and maintenance, including wing and empennage access.

The fuselage frame contains formers, pressure bulkheads, stressed skin and stringers.

Smoke detector and fire detection loops ensure the fire detection in the cargo bay. In case of the cargo bay fire, the cargo cabin altitude is lowered to suppress the fire until landing. The second deck cabin air is conditioned separately from cargo cabin air.

1.2.3. Tail Unit

The tail unit consists of vertical and horizontal parts.

The horizontal part includes two stabilizer sections and two elevators. Each elevator consists of inner and outer part. The structure of horizontal stabilizer includes two spars, stressed skin and stringers. Elevators are aerodynamically balanced and is trimmable via trim tabs. Anti-icing system, powered by the compressor bleed air, ensures the absence of ice on the stabilizer surface.

The vertical stabilizer includes fin and rudder. The structure of the fin consists of two spars, stressed skin and stringers. The rudder is aerodynamically balanced and is trimmable via trim tabs.

Vertical and horizontal stabilizers' sweep is greater than the wing sweep in order to ensure that in case of increase the Mach number up to critical values aerodynamic capabilities of the tail unit hold longer than those of the wing to ensure controllability of the aircraft.

The tail unit has conventional design, providing adequate maneuverability and eliminating the possibility of "deep stall" that is characteristic for the T-tail design, popular among lot of cargo aircraft. Moreover, such design is easier in maintenance due to its low position and it is lighter.

1.2.4. Landing gear

Landing gear consists of two parts: nose LG and main LG.

Nose LG incorporates two LG struts with two wheels on each strut. It has telescopic design. Nose LG allows the aircraft to steer on the ground, supports the aircraft on the ground and absorbs the shock on landing. The gear struts are attached to the forward part of the main fuselage, but the retraction happens forward into the LG bay in the forward part of the nose.

Main LG incorporates five LG struts on each side of the fuselage with two wheels on each strut. It provides the main support on the ground, wheel braking and absorbs the landing shocks. It is also possible to lower the aircraft, tilting it forwards, to provide easy access to the forward ramp. This process is called "kneeling". The main LG retracts into the bays on the fuselage sides.

LG retraction, extension and "kneeling” are provided by the usage of hydraulic actuators. In the landing gear bays, most part of the hydraulic system units is located. Fire detection loops in the bays provide warnings to the cabin in case of fire.

1.2.5. Engines

The aircraft is equipped with 4 turbofan engines. Such engine choice is based on the transonic speed and cruise altitude of 9 km, as this engine type is much more efficient than turboprop for such flight regimes. The number of engines meets thrust requirements without needing too powerful engine and allows flight in abnormal situations with one or two engine failures. The engines are installed on underwing pylons to ensure ease of maintenance and load the wing. Two fire detection loops in each engine provide overheat and fire detection and cabin warnings. Engine fire extinguishing is provided by 4 Halon bottles with squibs.

Engine compressor bleed air goes to the air conditioning and anti-icing systems and shafts driven by accessories gearbox, drive the electrical generators and hydraulic pumps.

In the case of the absence of engine power, it is possible to use the power from two APUs, installed in the main LG bays.

4 power plants of the Pratt & Whitney PW4000 – 112 type are chosen. The engines features are such:

- Compressor includes a fan, 6-stage low pressure compressor, 11-stage high pressure compressor;
- Annular combustor;
- Turbine includes 2 stages of high pressure and 7 stages of low pressure.

The engine's performances are presented in table 1.2.

Table 1.2

Engine performances

Take-off thrust, kN	Fan diameter, mm	Bypass ratio	Pressure ratio	Dry weight	Fan pressure ratio
408	2840	6.4	40	7140	1.8

The engine is a modern powerful unit with low fuel consumption and high power. It is rather reliable and was not involved in any major accidents after the fix of turbine blades problems.

1.3. Geometrical calculations of the aircraft main parts

The aircraft layout and geometry are determined by a number of factors, such as aerodynamic characteristics, aircraft's role, operational conditions, designed flight performances (range, cruise speed, etc.) and many others.

The layout calculations include sizing and disposition of all main units and loads to best meet all of the requirements. The calculation is performed by standard procedure described in [1]. The data for calculation is given in Appendix A.

1.3.1. Wing geometry calculation

Full wing area is:

$$S_w = \frac{m_0 \cdot g}{6099} = 1019 \ \text{m}^2,$$

where m_0 – the MTOM, kg; g – the gravity acceleration, m/s^2; P_0 – specific wing load, N/m^2.

Wing span is:

$$l_w = \sqrt{S_w \cdot \lambda_w} = \sqrt{1019 \cdot 8.6} = 94 \ \text{m},$$

where λ_w – the aspect ratio of the wing.

The root chord is:

$$b_0 = \frac{2S_w \cdot \eta_w}{(1+\eta_w) \cdot l_w} = \frac{2 \cdot 1019 \cdot 3.04}{(1+3.04) \cdot 94} = 16.3 \text{ m},$$

where η_w – the taper ratio of the wing.

The tip chord is:

$$b_t = \frac{b_0}{\eta_w} = \frac{16.3}{3.04} = 5.36 \text{ m}$$

As the wing has trapezoidal shape, the on-board chord length may be calculated and its value is:

$$b_b = b_0 \cdot \left(1 - \frac{(\eta_w - 1) \cdot D_f}{\eta_w \cdot l_w}\right) = 16.3 \cdot \left(1 - \frac{(3.04-1) \cdot 8.4}{3.04 \cdot 100}\right) = 15.4 \text{ m},$$

where D_f – the fuselage diameter.

It is required to determine the internal design of the wing to choose its loading scheme. As the wing has rather significant dimensions and supports high load, four-spar scheme is, while unusual, the most suitable choice for ensuring the structural integrity of such enormous construction.

The mean aerodynamic chord length was determined by the geometrical method as it allows simply and accurately determine the value.

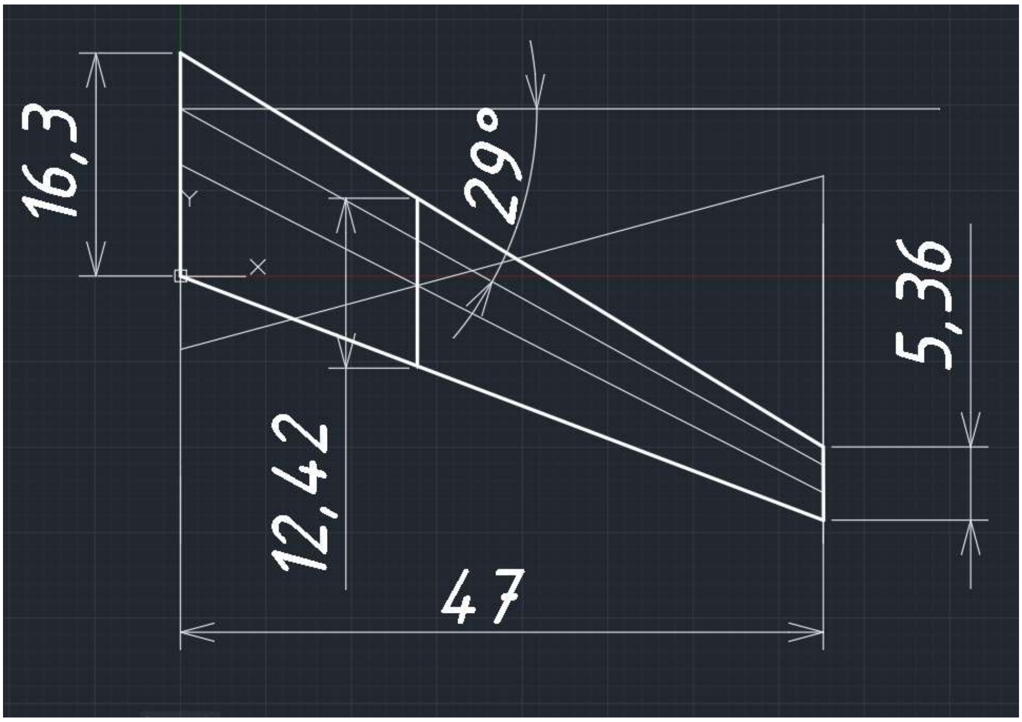

Fig. 1.1. Mean aerodynamic chord determination by geometrical method.

Therefore, the mean aerodynamic chord is 12.42 m.

Now it is required to calculate the main parameters of control surfaces. Ailerons geometrical parameters are determined as:

Ailerons span:

$$l_{ail} = (0.3...0.4) \cdot \frac{l_w}{2} = 0.38 \cdot \frac{94}{2} = 18 \text{ m}.$$

Aileron chord:

$$b_{ail} = (0.2...0.26) \cdot b_t = 0.25 \cdot 5.36 = 1.34 \text{ m}.$$

Aileron area:

$$S_{ail} = (0.05...0.08) \cdot \frac{S_w}{2} = 0.72 \cdot \frac{94}{2} = 33.9 \text{ m}^2.$$

The values are in accordance with the established proportions of similar aircrafts. They are optimal in the context of balance, maneuverability and required lift increase by high lift devices. The aileron chord length is restricted by location of the rear spar of the wing torsion box.

Aerodynamic balance of the ailerons is:

$$S_{ax.ail} = 0.266 \cdot 33.9 = 9 \text{ m}^2.$$

For four-engined aircraft trim tab area is:

$$S_{tt} = (0.04...0.06) \cdot S_{ail} = 0.05 \cdot 33.9 = 1.695 \text{ m}^2.$$

Upward aileron deflection is 25 degrees and downward is 15 degrees.

1.3.2. Fuselage layout

For a cargo aircraft, the fuselage layout consists of the layout of cargo cabin and the accommodation of the load masters and the crew needs.

For the cargo cabin, it is required to determine the desired cargo type and the purpose of the transportation and choose the appropriate cargo cabin dimensions, loading means and attachment points. For the crew needs, it is required to determine the seating quantity, lavatories and galleys location.

However, first of all it is required to determine the fuselage geometry:

Length of the fuselage is:

$$L_f = D_f \cdot \lambda_f = 8.4 \cdot 10 = 84 \text{ m},$$

where λ_f –fuselage fineness ratio.

Length of the forward part of the fuselage is:

$$L_{np} = D_f \cdot \lambda_{np} = 8.4 \cdot 1.35 = 11.34 \text{ m},$$

where λ_{np} –fuselage fineness ratio.

Length of the rear part of the fuselage:

$$L_{rp} = D_f \cdot \lambda_{rp} = 8.4 \cdot 3 = 25.2 \text{ m},$$

where λ_{rp} –fuselage fineness ratio.

Now it is possible to determine the cargo cabin parameters. It is designed to carry various types of loads, including unusual cargo such as other aircraft parts or vehicles. The cargo cabin takes all of the lower deck of the aircraft. It has two cargo entrances. The first is through the nose ramp, which may be accessed by rotating upwards the nose of the fuselage and extending the nose ramp. The second is by the tail ramp, which may be accessed by opening the hatch in the rear cone of the fuselage. The dimensions of the nose ramp, cargo cabin and tail ramp are given in the layout drawing. In the flight, the nose and tail ramps are closed and serves as the pressure bulkheads for the fuselage. On the ramps, monodirectional rollers are installed to simplify the cargo movement to the cabin.

On the cargo cabin floor, 9 rows of attachment points for straps, chains and other locking devices are provided. They are uniformly distributed along whole surface of the floor to provide attachment for the most untypical cargo. The loading equipment and tools are distributed among various storage units along the cabin and on the second deck. To simplify the cargo movement inside the cabin, 6 rows of ball rollers are installed. Two overhead cranes are provided to move the cargo into and inside the cabin. The floor is reinforced to withstand high loads that may happen in usage.

The second deck is designed to accommodate the cockpit, load masters and the equipment for loading. It is divided into two parts by the center wing box. In both parts 12 seats for load masters and other cargo companions, one lavatory and one galley are provided. The access to the decks is by the floor hatches and retractable ladders. Door to the cockpit is installed in the forward part. Emergency exits with ropes are provided in the sides of the upper deck and the cockpit window for the events of cargo fire. In the available space, storage units for emergency equipment, cargo loading equipment and other miscellaneous items is provided.

1.3.3. Tail unit design

The tail unit is of conventional type, based on the existing practices in prototype design, and the on the fact that such scheme requires less structural elements and control linkages, which optimizes both weight and economic efficiency of the aircraft.

The geometrical dimensions of the stabilizers and control surfaces are determined below.

Vertical tail unit parameters are the next:

Area of vertical tail is:

$$S_{VTU} = \frac{l_w \cdot S_w}{L_{VTU}} \cdot A_{VTU} = \frac{94 \cdot 1019}{40} \cdot 0.07 = 168\ \mathrm{m}^2,$$

where L_{VTU} – the arm of horizontal tail unit, m (it is taken proportionally to the value of prototypes); A_{VTU} – the coefficient of static moments assumed as 0.07 in the range provided by the methodical guide.

Height of the vertical tail unit is:

$$h_{VTU} = (0.13...0.165) \cdot l_w = 0.166 \cdot 94 = 15\ \mathrm{m}.$$

Tip chord of the vertical tail unit is:

$$b_{tipVTU} = \frac{2S_{VTU}}{(1+\eta_{VTU}) \cdot h_{VTU}} = \frac{168 \cdot 2}{(3.29+1) \cdot 15} = 5.2\ \mathrm{m},$$

where η_{VTU} – the vertical tail unit taper ratio chosen based on prototype performances.

MAC of the vertical tail unit is:

$$b_{MACVTU} = 0.66 \cdot \frac{\eta^2_{VTU} + \eta_{VTU} + 1}{\eta_{VTU} + 1} \cdot b_{tipVTU} = 0.66 \cdot \frac{3.29^2 + 3.29 + 1}{3.29 + 1} \cdot 5.2 = 10.5\ \mathrm{m}.$$

Root chord of the vertical tail unit is:

$$b_{rootVTU} = b_{tipVTU} \cdot \eta_{VTU} = 5.2 \cdot 3.29 = 17.1\ \mathrm{m}.$$

Horizontal tail unit parameters are the next:

Area of the horizontal tail unit is:

$$S_{HTU} = \frac{b_{MAC} \cdot S_w}{L_{HTU}} \cdot A_{HTU} = \frac{12.42 \cdot 1019}{42} \cdot 0.55 = 166\ \mathrm{m}^2,$$

where L_{HTU} – the arm of horizontal tail unit, m (and is taken proportionally to the value of prototypes); A_{HTU} – the coefficient of static moments assumed as 0.55 in the range provided by the methodical guide.

Span of the horizontal tail unit is:

$$l_{HTU} = (0.32...0.5) \cdot l_w = 0.36 \cdot 94 = 33.8 \text{ m}.$$

Tip chord of the horizontal tail unit is:

$$b_{tipHTU} = \frac{2S_{HTU}}{\left(1+\eta_{HTU}\right) \cdot l_{HTU}} = \frac{2 \cdot 166}{(1+2.8) \cdot 33.8} = 2.6 \text{ m},$$

where η_{HTU} – the horizontal tail unit taper ratio chosen based on prototype performances.

MAC of the horizontal tail unit is:

$$b_{MACHTU} = 0.66 \cdot \frac{\eta^2_{HTU} + \eta_{HTU} + 1}{\eta_{HTU} + 1} \cdot b_{tipHTU} = 0.66 \cdot \frac{2.8^2 + 2.8 + 1}{2.8 + 1} \cdot 2.6 = 5.26 \text{ m}.$$

Root chord of the horizontal tail unit is:

$$b_{rootHTU} = b_{tipHTU} \cdot \eta_{HTU} = 2.6 \cdot 2.8 = 7.28 \text{ m}.$$

Elevators area is:

$$S_{el} = (0.3...0.4) \cdot S_{HTU} = 0.3 \cdot 196 = 58.8 \text{ m}^2.$$

Elevators aerodynamic balance area is:

$$S_{abel} = (0.18...0.2) \cdot S_{el} = 0.19 \cdot 58.8 = 11.172 \text{ m}^2.$$

Elevators trim tab area is:

$$S_{te} = (0.08...0.12) \cdot S_{el} = 0.1 \cdot 58.8 = 5.88 \text{ m}^2.$$

Rudder area is:

$$S_{rud} = (0.2...0.22) \cdot S_{VTU} = 0.2 \cdot 168 = 33.6 \text{ m}^2.$$

Rudder aerodynamic balance area is:

$$S_{abrud} = (0.18...0.2) S_{rud} = 0.2 \cdot 33.6 = 6.72 \text{ m}^2.$$

Rudder trim tabs area is:

$$S_{tr} = (0.08...0.12) \cdot S_{rud} = 0.1 \cdot 33.6 = 3.36 \text{ m}^2.$$

1.3.4. Landing gear design

For the preliminary design of the aircraft it is required to calculate the location of the landing gear struts relatively to the center of gravity and to each other. Also it is important to locate the landing gear in such way that it will fit the airports standard taxiways and hangars and will be convenient for operation and maintenance.

The distance from the centre of gravity to the main LG is:

$$B_m = (0.15...0.2) \cdot b_{MAC} = 0.16 \cdot 12.42 = 2 \text{ m.}$$

The distance is not too large to provide the lifting of the nose gear but large enough to prevent the tail-strike during take-off and to provide enough load to the nose LG to increase stability.

Landing gear wheel base is:

$$B = (0.3...0.4) \cdot L_f = 0.38 \cdot 84 = 32 \text{ m.}$$

The distance from the center of gravity to the nose LG is:

$$B_n = B - B_m = 32 - 2 = 30 \text{ m.}$$

As the main LG is installed on the sides of the fuselage to provide easier loading and unloading of the aircraft, the wheel track is restricted by the fuselage geometry and is equal to 8.6 m.

Nose wheel load is:

$$F_{nose} = \frac{B_m \cdot m_0 \cdot 9.81 \cdot K_g}{B \cdot z} = \frac{2 \cdot 633326 \cdot 9.81 \cdot 1.5}{32 \cdot 2 \cdot 2} = 145615 \text{ N} = 32735 \text{ lbs},$$

where n – the quantity of supports, z – the number of wheels on one leg and K_g = 1.5…2.0 – the dynamics coefficient. The value is converted to lbs for compliance with the standard manufacturer's catalogs.

Main wheel load is:

$$F_{main} = \frac{(B - B_m) \cdot m_0 \cdot 9.81}{B \cdot n \cdot z} = \frac{(32 - 2) \cdot 633326 \cdot 9.81}{32 \cdot 10 \cdot 2} = 291231 \text{ N} = 65471 \text{ lbs},$$

where n – the quantity of supports and z – the number of wheels on one leg. The value is converted to lbs for compliance with the standard manufacturers' catalogs.

According to the calculated values of wheel loading and the take-off speed, the tires are selected from manufacturers catalog [2].

For the nose landing gear, Flight Leader 416K42-1 are chosen with rated load of P_{rated} = 33650 lbs, rated speed V_{rated} = 362 km/h, size H42×16.0-19.

For the main landing gear, Flight Leader 542K69-4 are chosen with rated load of P_{rated} = 68500 lbs, rated speed V_{rated} = 378 km/h, size 54×21.0-23.

The rate of wheel loading is:

- for nose wheel: $\frac{33650-32735}{33650}\cdot 100\% = 2.72\%$;
- for main wheel: $\frac{68500-65471}{68500}\cdot 100\% = 4.42\%$.

The values are inside the 10% limit. Therefore, such tires are allowable for usage.

1.4. Determination of the aircraft center of gravity position

1.4.1. Determination of centering of the equipped wing

The wing weight includes its own structure weight, weight of all of the equipment located inside of wing and the fuel mass in the tanks. Additionally, the main and the front landing gear are also included in the list of equipped wing masses even while they are actually attached to the fuselage. The list includes the object names, their masses in and the coordinates of their center of gravity, which are expressed in meters from the origin. The origin is chosen to be the most forward point of the Mean Aerodynamic Chord for the XOY plane. The positive direction of coordinate axis is towards the rear part of the fuselage. This is in accordance with [1]. Appendix B shows the locations of all masses in the wing.

Table 1.3 shows the list of all of the mass objects for the equipped wing. The coordinates for the equipped wing are found by the formulas:

$$X'_w = \frac{\sum m'_i x'_i}{\sum m'_i},$$

where X'_w – the center of mass of equipped wing, m; m'_i – mass of a unit, kg; x'_i – the center of mass of a unit, m.

Table 1.3

List of equipped wing masses

Object name	Unit mass	Mass, kg	CG coordinates, m	Moment of mass, kg·m
Wing (structure)	0.1032	65353	5.589	365257.41
Fuel system, 80-100%	0.0082	5193	4.471	23220.16
Control system, 30%	0.0007	456	7.452	3398.07
Electrical equipment, 20%	0.0006	367	1.242	456.22
Anti-icing system, 70%	0.0020	1237	1.242	1536.21
Hydraulic system, 30%	0.0024	1539	7.452	11468.50
Power plant	0.0845	53516	0.310	16589.97
Equipped wing without landing gear and fuel	0.2016	127661	3.305	421926.55
Nose landing gear	0.0112	7062	-26.144	-184618.08
Main landing gear	0.0335	21185	5.157	109249.78
Fuel for flight	0.1979	125361	3.726	467093.40
Reserve fuel	0.0357	22622	4.347	98339.59
Totally equipped wing	0.4798	303891	3.001	911991.26

1.4.2. Determination of the centering of the equipped fuselage

The origin for the coordinates of fuselage equipment is chosen to be the nose of the fuselage on the horizontal axis. The list of the equipped objects on the fuselage is given in the table 1.4. Appendix C shows the locations of all masses in the fuselage.

The CG coordinates are determined by formula:

$$X_f = \frac{\sum m'_i X'_i}{\sum m'_i},$$

where X'_w – the center of mass of equipped fuselage, m; m'_i – mass of a unit, kg; x'_i – the center of mass of a unit, m.

Table 1.4

List of equipped fuselage masses

Object name	Unit mass	Mass, kg	CG coordinates, m	Moment of mass, kg·m
1	2	3	4	5
Fuselage	0.0874	55321	42.000	2323483.10
Horizontal tail unit	0.0093	5858	79.334	464759.64
Vertical tail unit	0.0092	5827	77.055	448968.60

Ending of table 1.4

1	2	3	4	5
Radiolocation equipment	0.0010	633	1.000	633.33
Dashboard and instrument equipment	0.0018	1140	6.000	6839.92
Aero navigation equipment	0.0015	950	6.000	5699.93
Radio equipment	0.0008	507	9.000	4559.95
Fuel system, 0-20%	0	0	0	0.00
Control system, 70%	0.0017	1064	46.200	49156.23
Electrical system, 80%	0.0023	1469	42.000	61711.29
Hydraulic system, 70%	0.0057	3591	37.220	133655.47
Anti-icing system, 30%	0.0008	530	77.756	41217.98
Air-conditioning system	0.0065	4123	37.800	155847.60
Emergency equipment	0.0008	500	38.500	19250.00
Tools	0.0011	700	30.000	21000.00
Water and liquid	0.0005	300	18.000	5400.00
Lavatory 1	0.0002	100	18.000	1800.00
Lavatory 2	0.0002	100	48.000	4800.00
Galley 1	0.0003	200	12.000	2400.00
Galley 2	0.0003	200	54.000	10800.00
Cargo loading equipment	0.0632	40000	37.300	1492000.00
Interior panels, lining and insulation	0.0041	2597	37.800	98152.86
Pilots' seats	0.0001	50	7.800	390.00
Flight attendants' seats	0.0003	160	35.000	5600.00
Non-typical equipment	0.0045	2869	37.300	107012.46
Equipped fuselage without commercial load	0.2034	128789	42.435	5465138.35
Cargo, mail	0.3158	200000	37.300	7460000.00
On board meal	0.0000	10	12.000	120.00
Flight attendants	0.0005	320	14.000	4480.00
Crew	0.0005	320	7.800	2496.00
Totally equipped fuselage	0.5202	329439	39.255	12932234.35

After determination of wing and fuselage equipped masses, the moment equilibrium equation relatively to the fuselage nose is constructed:

$$m_f \cdot X'_f + m_w (X_{MAC} + X'_w) = m_0 (X_{MAC} + C),$$

where m_0 – aircraft take-off mass, kg; m_f – mass of fully equipped fuselage, kg; m_w – mass of fully equipped wing, kg; C – distance from MAC leading edge to the center of gravity point.

Then, MAC leading edge position relative to fuselage X_{MAC} value by formula:

$$X_{MAC} = \frac{m_f \cdot X'_f + m_w \cdot X'_w - m_0 \cdot C \cdot b_{MAC}}{m_0 - m_w},$$

$$X_{MAC} = \frac{329439 \cdot 39.255 + 303891 \cdot 3.001 - 633326 \cdot 0.3}{633326 - 303891} = 34.861 \text{ m.}$$

1.4.3 Calculation of center of gravity positioning variants

The list of all equipped masses for calculation given in table 1.5 and the center of gravity calculation options are given in table 1.6, which are created on the basis of table 1.3 and table 1.4.

Table 1.5

Calculation of CG coordinates

Object name	Mass, kg	CG coordinates, m	Moment of mass, kg·m
Equipped wing without landing gear and fuel	127661	38.166	4872335.04
Nose landing gear (extended)	7062	8.717	61556.04
Main landing gear (extended)	21185	40.018	847772.12
Fuel for flight	125361	38.587	4837291.08
Reserve fuel	22622	39.208	886979.89
Equipped fuselage	128789	39.255	5055648.18
Cargo, mail	200000	37.300	7460000.00
On board meal	10	12.000	120.00
Flight attendants	320	14.000	4480.00
Crew	320	7.800	2496.00
Nose landing gear (retracted)	7062	8.016	56605.87
Main landing gear (retracted)	21185	40.018	847772.12

Table 1.6

Aircraft's CG position variants

Variant of loading	Mass, kg	Moment of mass, kg·m	CG coordinates, m	Centering, %
Take-off mass (landing gear extended)	633329	24028678.34	37.940	24.79
Take-off mass (landing gear retracted)	633329	24023728.17	37.932	24.73
Landing variant (landing gear extended)	507959	19191267.27	37.781	23.51
Transportation variant (without payload)	432999	16559128.17	38.243	27.23
Parking variant (without fuel and payload)	284697	10837311.38	38.066	25.81

Conclusions to the project part

The aircraft designed during the course project is suitable for the planned purpose. Furthermore, during the calculations it was found that the payload may be even increased to 200000 kg due to removal of excessive weight of operational items which were calculated automatically.

Operational purpose, planned cargo weight, cruise speed, altitude and runaway conditions were all considered during the calculations. The calculation include:

- The geometry and positions of the principal units of the aircraft;
- The cargo cabin layout and equipment for 200000 kg payload;
- The aircraft center of gravity calculations;
- The choice of wheels that satisfy the requirements;
- The landing gear design;
- The choice of power plant.

During the centering the location of center of gravity relative to the MAC position was determined. The most forward of the position is 23.51% of the MAC in the landing variant and the most aft position is 27.23% of the MAC in the transportation variant. Both of these values are inside the average statistical range for the high-wing aircraft.

Finally, the chosen engine Pratt & Whitney PW4000-112 is suitable for required thrust requirements for the design.

Using the results of calculations, drawings of the designed aircraft were made, mainly based on the An-124 prototype.

2. ANALYSIS OF FATIGUE CRACK GROWTH DEPENDACIES

2.1 The problems of fatigue damage in aviation

All aircraft are subjected to repeated loads of various nature. These include cycles of pressurization, loading and unloading by cargo, loading by wing gusts, maneuvers, vibrations from engines, landing shocks and unevenness and others. Fig. 2.1. shows an example of the load spectrum for an aircraft component for only one flight.

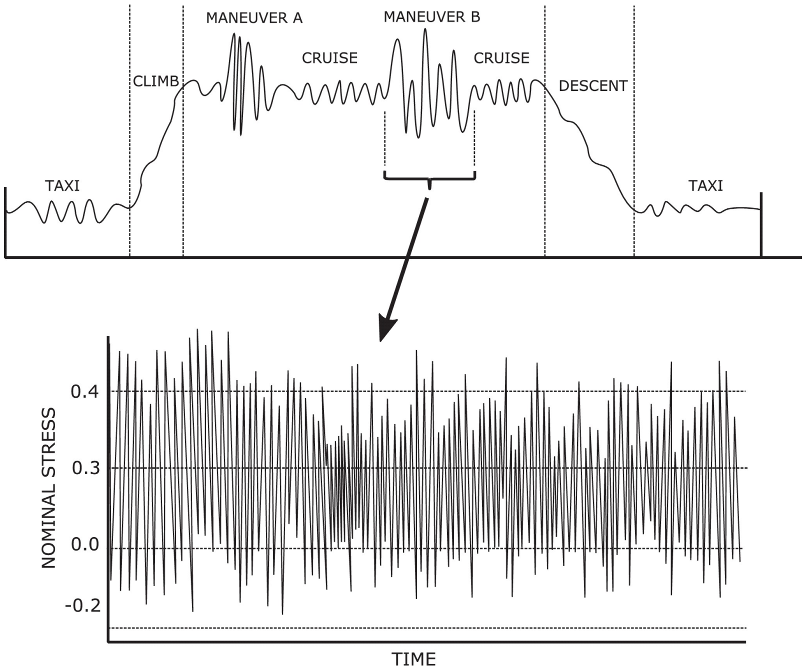

Fig. 2.1. Typical load spectrum for a structural component of an aircraft during one flight [4].

All of these cycles of loading of various structural members cause the process that is called fatigue. Fatigue is a process of cumulative decrease of the strength of a component in operation while subjected to stresses that are significantly lower than the ultimate strength of the component. The fatigue crack initiation may happen in the places of stress concentrations due to microstructure irregularities, bad design or low manufacturing quality [3,4].

There are few widely accepted approaches for fatigue design. The first approach is so-called "safe-life" design, where the component is designed in such way that critical failure will not happen over some pre-determined period of operation. It is important to understand that it does not mean that this period will correspond to the expected service life of the whole aircraft – it only means that the detail has to be replaced as part of maintenance before this period ends. This approach is not very cost-efficient, as it underutilizes the material strength as the detail will be often replaced without not just critical, but any damage. Moreover, the costs of implementing such strategy is rather high as it calls for complete replacement of a component which is an expensive process [5]. However, this approach is actually still used nowadays for some parts that are hard to inspect and are critical structural parts, such as landing gear, major wing joints and fuselage-wing joints [3].

The second approach is the fail-safe approach, according to which the structure is designed in such way that the failure of a member does not lead to the complete failure of the structure. This is achieved by making the structure redundant using multiple load paths, incorporating crack stoppers and other features. To prevent complete failure, the structure should be repeatedly inspected for the presence of cracks and repairs should be made in case of crack existence. This approach is more efficient as the detail's strength will be fully used and the details themselves will generally be lighter [3,5].

As the NDT methods developed into more modern, a special sub-approach appeared from fail-safe approach, called damage tolerance. Sources vary as to whether it is a unique approach or just natural development of fail-safe approach, but, for example, FAR Amendment 25-72 states that damage tolerance emphasizes inspection and repair of the cracks before they grow to critical sizes, while fail-safe emphasizes designing detail in such way that even large cracks will not completely hinder component operation [6]. Therefore, damage tolerance employs inspections of regular character to provide safety in operation. It leads to two requirements: to provide high accessibility for the inspected parts and to determine the frequency the inspections. Nonetheless, even with the problems of high workload on inspections, damage tolerance is the preferred method of aircraft components design where it is possible, as it provides high efficiency, structure lightness – so it is the most economical approach.

Modern approaches include two considerations of the design that incorporates fatigue. The first is the provision of structural durability, the ability of the structure to sustain degradation from various factors (which include fatigue, corrosion, accidental damage etc.). This quality mainly influences economic efficiency of the aircraft, as while it is possible to ensure absence of any damage by making inspections and repairs practically as often as it is needed, such process will be extremely expensive and will remove any gains from the aircraft. Therefore, wise design choices are made based on various methods of durability predictions, which include testing the materials for cycles to rupture on various stress amplitudes and approximating the data, using empirical data and coefficients to calculate details expected life, computer-based simulations and even full-scale tests. After this, design objectives for some minimal damage-free lives are determined. It is estimated that inconsistency in design between the expected life on some stresses amplitude and the operating stresses caused over 85% of encountered fatigue-related problems [7,8].

The second consideration is, interestingly enough, to provide damage tolerance itself. Actually, the name of the approach comes from this quality, as it is the ability to sustain the loads when there is some damage present for enough time that it will be possible to detect it during inspection and repair. This consideration is actually mostly regulated by certification standards. Damage tolerance consideration itself may be divided into three equally important elements:

1. Damage detection – regular inspections of the aircraft that will allow to detect the damage in time.
2. Residual strength – making sure that the structure with presence of damages up to pre-determined critical size (including the possibility of multiple simultaneous damages) is able to withstand the limit loads.
3. Crack growth – making sure that the crack will not grow too rapidly between the inspections [8].

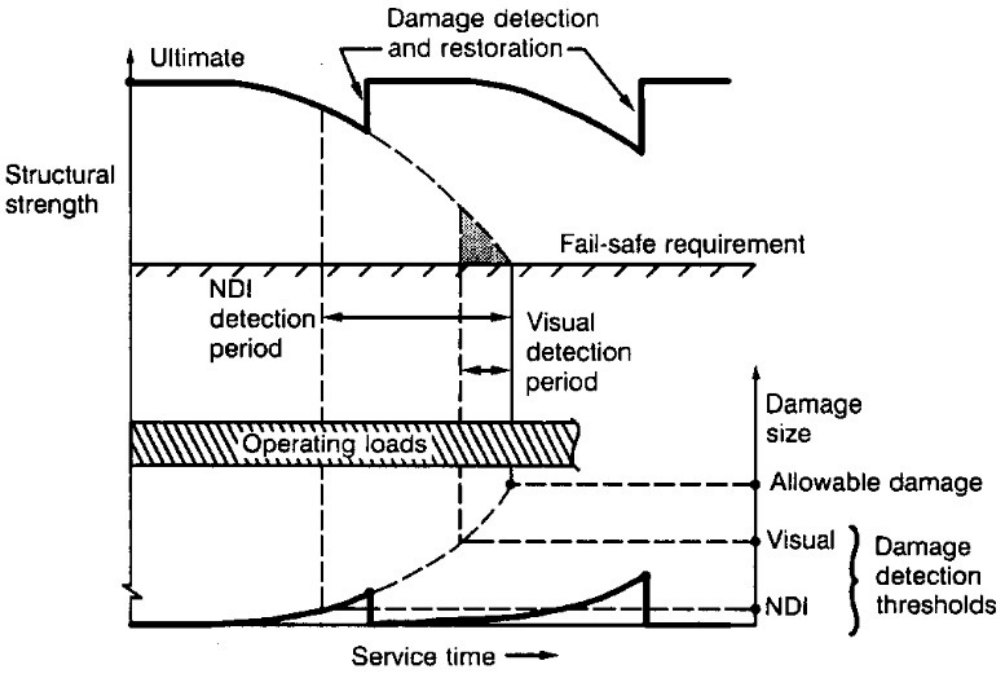

Fig. 2.2. The operation of damage-tolerant structure [8].

Therefore, it is extremely important to study the processes of crack growth in aviation materials to ensure that cracks will not reach critical size in operation before NDT will be able to detect it. However, while static failure is a process mostly unaffected by random processes, fatigue failure has a stochastic nature that the results of the same experiment will vary and the same parts may and will fail at significantly different times. That means that to get meaningful results it is not enough to do singular test of the material sample – large samples sizes have to be studied and probability of different outcomes must be derived. Also that means that full-scale tests of a assembly or even the whole aircraft are not viable as singular sources of information (although they are definetely important part of fatigue testing) – statistical data should be gathered on each stage of design and operation. Therefore, the study of dependancies of crack growth is a very important and relevant topic and such study based on the results of real tests is chosen to be the topic of this part of the work.

2.2. The experiment procedure

For the purpose of the analysis of the fatigue crack growth the samples made of sheets of aluminum alloy 1163ATB were chosen. A Western analogue of 1163 is an

Al2524 T3 alloy. 2524 is a duraluminum series alloy that is characterized by high fracture toughness and durability and medium strength which can be used in the form of sheets for skin of the fuselage, lower wing surface or as extruded profile for stringers in the same areas. Due to the fact that its fatigue-resistive properties are higher than ones of 2024 series alloys (15-20% better fracture toughness, twice better fatigue crack growth resistance and 30-40% loner time to failure with practically same strength and corrosion resistance), it is widely used for the details that are critical by fatigue in tensile zones [10].

The chemical composition of 2524 alloy is presented in table 2.1 [10].

Table 2.1

Chemical composition of 2524 alloy

Chemical composition, %										
Al	Cr	Cu	Fe	Mg	Mn	Si	Ti	Zn	Other, each	Other, total
92.5-94.4	≤0.05	4-4.5	≤0.12	1.2-1.6	0.45-0.7	≤0,06	≤0.1	≤0.15	≤0.05	≤0.15

The mechanical properties of Al2524-T3 alloy are presented in table 2.2 [9,10].

Table 2.2

Mechanical properties of 2524-T3 alloy

Density, g/cm^3	Yield stress, MPa	Ultimate stress, MPa	Total strain, %	Young modulus, GPa	Hardness by Brinnel
2.78	320	436	17	72	130

The material is cladded by layer of a pure aluminum to improve corrosion resistance and age hardened to improve strength.

For the purpose of this test, middle tension specimens were used. Such specimen is a sample with a center crack that can be loaded by both positive and negative R-ratios, either for tension-tension or tension-compression cycles. All dimensions, manufacturing details and test procedures that are described further are in accordance with ASTM E647-15e1 "Standard Test Method for Measurement of Fatigue Crack Growth Rates" [11].

The center crack originates from a stress concentrator in the centre of the specimen. The concentrator is machined in a shape of through hole with a transverse notch, as shown on fig. 2.3.

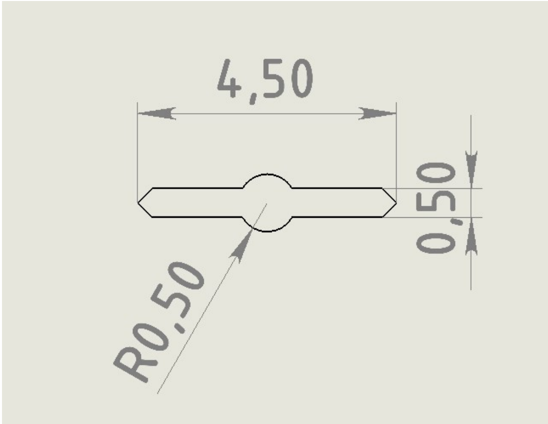

Fig. 2.3. Dimensions of the stress concentrator.

A straight crack of length of 1.5 mm is pre-grown in such way that the stress intensity factor value K during this process is less then the initial value of stress intensity factor which will be recorded during the experiment. It is done to eliminate the effect from the machined notch on the value of the factor and to not include the early stages of crack initiation in the test results. It is very important not to exceed mentioned above level of K as if there is decrease of K during the experiment, it may influence the results at near-criticial state.

Test samples are then clamped into testing machine and are loaded with σ_{max} = 10 kgf/mm^2, R = 0.2 until the crack reaches pre-determined ending length. The ending length is determined by the requirements for the test of residual strength, which are not covered in this work.

The peculiarity of these experiments lies in the fact that the samples were not always made from the new material. For the first test, brand-new sheet of size 3600×1200×1.5 (dimensions of loaded part) was created and tested. For the testing of such large specimen anti-buckling railings made of steel rods were installed. Between the railings and specimen, a film layer was installed to reduce the influence of friction. After the crack reached the pre-determined size, the specimen was statically destroyed to test its residual strength, after which 4 middle-cracked specimens of size 1800×600×1.5 were made from the leftover materials and tested similarly. As the process was repeated a couple more times, for the purpose of this work two-digit numbering system for samples will be employed. The first digit will represent the size of the sample; the second digit will be denoted as a Roman numeral and will represent the generation of the sample – showing which time the same material is tested.

The procedure of retesting samples of same material was actually used up to fourth generation of samples. In the third generation, one more sample group of the similar size, but produced from new material, was introduced for comparison of the test results. The sizing, number of samples, group names and generation may be found in table 2.3.

Table 2.3

Samples data

Group name	L, mm	W, mm	B, mm	Sequence	Samples quantity
1-I	3600	1200	1.5	New	1
2-II	1800	600	1.5	After 1-I	4
3-III	900	300	1.5	After 2-II	8
3-I	900	300	1.5	New	4
4-III	600	200	1.5	After 2-II	8
5-IV	300	100	1.5	After 3-III	8
5-II	300	100	1.5	After 3-I	8

As the largest stress intensity in the samples happens in the zone of the notch, it was hypothesized that pre-loading will not significantly impact crack growth and the data will be applicable for usage. This hypothesis will be checked further in the work.

The number of cycles N was registered by the data acquisition system of the testing machine itself.

For the further calculations, effective crack length a_{eff} (in later subchapters denoted as a for cluttering purposes) was used. Effective crack length includes visible crack length and plastic zone near crack tip. To determine a_{eff}, compliance method was used. Compliance is the change of the crack-opening displacement Δv divided by change in force carried by specimen during the test ΔP. To measure the crack-opening displacement, tensometric device was installed at the slot so that its knives touched the upper and lower surfaces of the slot as shown on fig. 2.4.

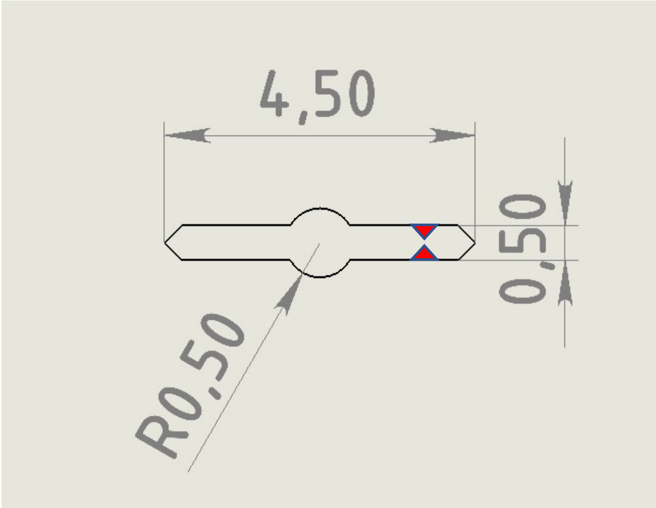

Fig. 2.4. Tensometric device knives application scheme.

Then, the values pairs were automatically linearly approximated and the slope was calculated. The slope than was put into empirical formulas to find effective crack length [11]:

$$X = 1 - \exp\left(\frac{-\sqrt{(EBC+\eta)(EBC-\eta)}}{2.141}\right);$$

$$a_{eff} = \frac{W}{2}\left(1.06905X + 0.588106X^2 - 1.01885X^3 + 0.36169X^4\right),$$

where E – the modulus of elasticity; B – the specimen thickness; c – the specimen compliance; W – the specimen width; η – non-dimensional gage length.

After that, data pairs of effective crack length a and respective cycles number N are presented.

For the analysis presented in this work, large data sets should be compared. Therefore, it makes sense to analyze the results of groups with 8 samples. Due to that fact, most attention will be foremost given to groups 5-IV and 5-II as they have 8 samples each. Groups 3-III and 3-I will also sometimes be used for comparison.

To check the correctness of the experiment, crack growth dynamics were approximated by exponential law using MS Office Excel for each test from groups 5-IV and 5-II. An example of received diagram for sample 1, group 5-IV is shown on fig. 2.5. The correlation coefficient for each approximation is presented in table 2.4.

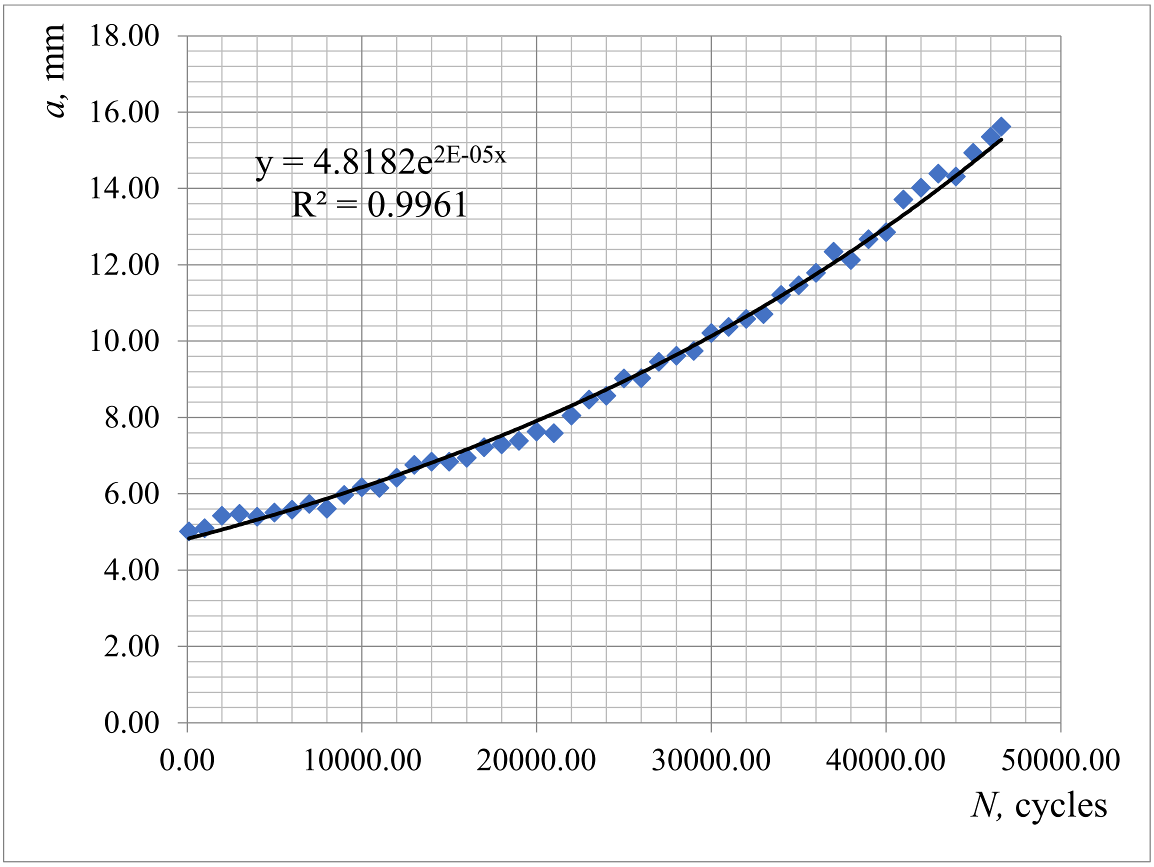

Fig. 2.5. Experimental data of crack growth for sample #1 from group 5-IV.

Table 2.4

Correlation coefficient R^2 for each sample

Sample #	Group 5-IV	Group 5-II
1	0.996	0.994
2	0.995	0.996
3	0.997	0.999
4	0.992	0.997
5	0.994	0.992
6	0.989	0.987
7	0.977	0.990
8	0.986	0.992

The coefficients prove that test results are relevant. Moreover, a tendency to slight less deviation is observed in group 5-II. The implications and possible reasons of this will be discussed further.

Based on the results, stress intensity coefficient for each point is calculated

$$\Delta K = \frac{\Delta P}{B}\sqrt{\frac{\pi\alpha}{2W}\sec\left(\frac{\pi\alpha}{2}\right)},$$

where $\Delta P = P_{max} - P_{min} = 1200$ kgf, $\alpha = 2a/W$ [11].

Then, crack growth rate da/dN was calculated as:

$$\frac{da}{dN} = \frac{a_{n+1} - a_n}{N_{n+1} - N_n}.$$

Finally, natural logarithms of stress intensity coefficient and crack growth rates were taken and the kinematic diagrams of crack growth were constructed, as shown in fig. 2.6-2.7.

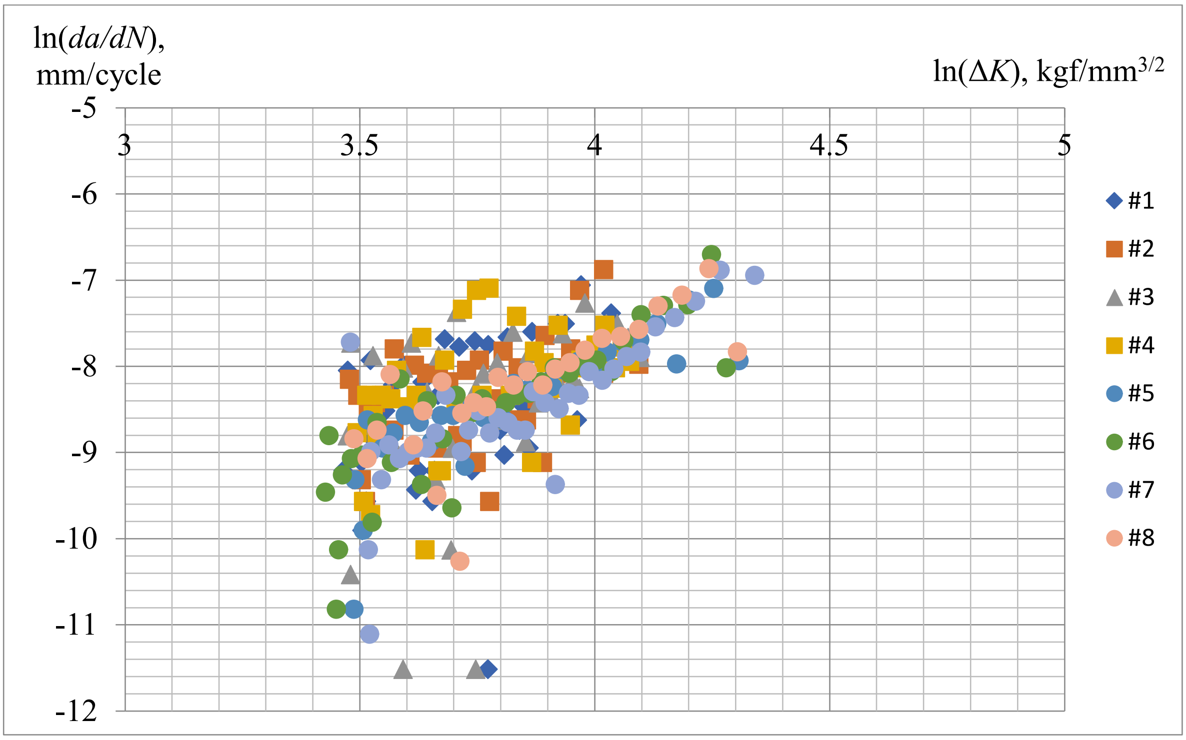

Fig. 2.6. Kinematic diagram of crack growth for test group 5-IV.

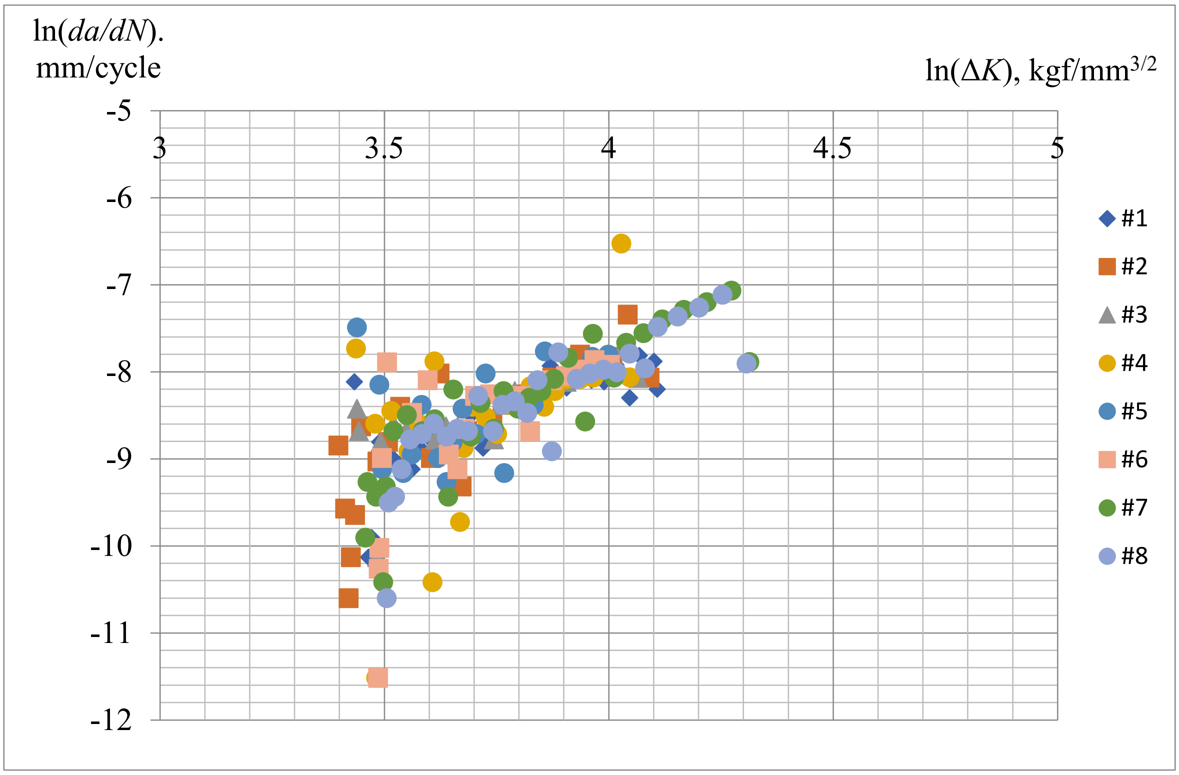

Fig. 2.7. Kinematic diagram of crack growth for test group 5-II.

As it may be seen, the diagrams in both cases are similar to classical shape with the exception that is the absence of sharp growth closer to the end of the test. This fact, however, is explained by the test procedure, as it was decided to perform test of residual strength of these samples, so the crack hadn't been grown to criticality – therefore stress intensity is not allowed to tend to its fracture toughness value. This allows to conclude about adequacy of the experiment and viability of usage obtained data for further analysis.

The last notable detail here is that data from test samples from group 5-II again tend to be less dispersed, while test data from samples from group 5-IV, especially from samples #2 and #4, has more cloud-like characteristics. The implications and possible reasons of this will be discussed further.

2.3. Fatigue tests data analysis

2.3.1. The mathematical basis for statistical analysis

As it was discussed in 2.1, it is extremely important to study fatigue crack growth processes to be able to provide damage tolerance, as it is required to make inspections regular enough so that cracks will not reach critical sizes. In order to be able to complete this task, a statistical analysis has to be performed and predictions based on its results should be made for some standard values of time and/or defect size.

To do that, it is required to know the probability of appearance of crack of some size of interest on each number of cycles and the probability for crack to grow to each size on some given number of cycles. For this, a distribution that describes the process has to be found. Two-parametric Weibull distribution is usually used to describe crack growth processes [7,8]. Therefore, the most attention will be paid to Weibull distribution application in the analysis. However, for comparison purposes normal and logarithmic normal distributions will be applied and conclusion about their applicability will be made.

To describe the probability of an event happening before some point in time, cumulative distribution function is used.

Weibull distribution's cumulative probability function is defined as:

$$F(N) = 1 - \exp\left[-\left(\frac{N}{\beta}\right)^{\alpha}\right], \tag{2.1}$$

where N – number of cycles; α – shape parameter; β – scale parameter.

It is also useful to describe the derivative of cumulative probability functions, that is the probability density.

Weibull distribution's probability density function is defined as:

$$f(N) = \frac{\alpha}{\beta}\left(\frac{N}{\beta}\right)^{\alpha-1} \exp\left(-\left(\frac{N}{\beta}\right)^{\alpha}\right). \tag{2.2}$$

To define coefficients for Weibull's distribution, the equation (2.1) is transformed in such way:

$$\ln[1 - F(N)] = \ln\exp\left(-\left(\frac{N}{\beta}\right)^{\alpha}\right);$$

$$\ln[1 - F(N)] = -\left(\frac{N}{\beta}\right)^{\alpha};$$

$$\ln\ln\left[\frac{1}{1-F(N)}\right]=\ln\left(\frac{N}{\beta}\right)^{\alpha};$$

$$\ln\ln\left[\frac{1}{1-F(N)}\right]=\alpha\ln(N)-\alpha\ln(\beta).$$

The only variable in this equation are the number of cycles N and $F(N)$ is the function of that variable. Therefore, in double logarithmic coordinates this function describes a straight line, where the left-hand side of the equation the ordinate and $\ln(N)$ is the abscissa.

However, it is possible to obtain such line from the experiments results alone. To do that, the crack size of interest is chosen and the number of cycles N when the size was reached is found from the test data for each sample. Then, the data is sorted from the smallest to the largest value and grouped into intervals of close sizes. Then the number of the results that fall into each interval is found and the probability of this event on the interval happening is found. Then by summing the probabilities up to each interval it is possible to obtain the empirical data pairs of $F(N)$ and N. From that, it is not hard to get empirical ordinates and abscissas of point that correspond to the line by logarithms. Then the data pairs are plotted and approximated as a straight line by the means of MS Excel. The straight line equation is given in the form:

$$y=kx+b$$

from which it is easy to obtain $\alpha = k$ and $\beta = \exp(b/\alpha)$. Then these coefficients are put into Excel's built-in WEIBULL function and the Weibull distribution's values of cumulative distribution function and probability density functions may be output.

A benefit of such method is that during this approximation it is also possible to obtain the value of R^2 which allows to determine how well the Weibull distribution describes the process. Finally, for the analysis of crack lengths on some stated number of cycles, the functions are swapped, and $F(a)$ is obtained.

Normal and logarithmical normal distributions are obtained via Excel functions entirely with their coefficients being their mean and standard deviation, which are found from the same sample data by AVERAGE and STDEV functions, the only difference being that for lognormal distribution they are applied to the logarithms of the data. The according values of cumulative distribution functions and probability density are found by Excel's functions NORMDIST and LOGNORMDIST.

As it was mentioned above, the results from groups 5-IV and 5-II are of the most interest for the purpose of this work, as they provide the largest test samples quantity that allows to get more realistic analysis results and to reduce the influence of randomness in the experiment while maintaining same geometry that allows for the comparison between the experiments. Therefore, the statistical analysis will be performed on the results of these samples.

2.3.2. Analysis of pre-determined crack length probability

2.3.2.1. Comparison on same generation

By the described above procedure, cumulative probability functions and probability density functions were approximated for three levels of crack growth. The levels were chosen to be 7 mm, 10 mm and 15 mm. Such choice is explained by the fact that an attempt to gain data from various periods of crack growth was made to analyze the dependencies of the distributions changing with crack length increase. The upper length limit was restricted by experiment procedure to perform the residual strength tests later (those tests are not covered in this work). The graphs of typical approximation result are shown on fig. 2.8-2.9. The graphs of all other results for group 5-IV may be found in Appendix D, fig. D.1-D.4.

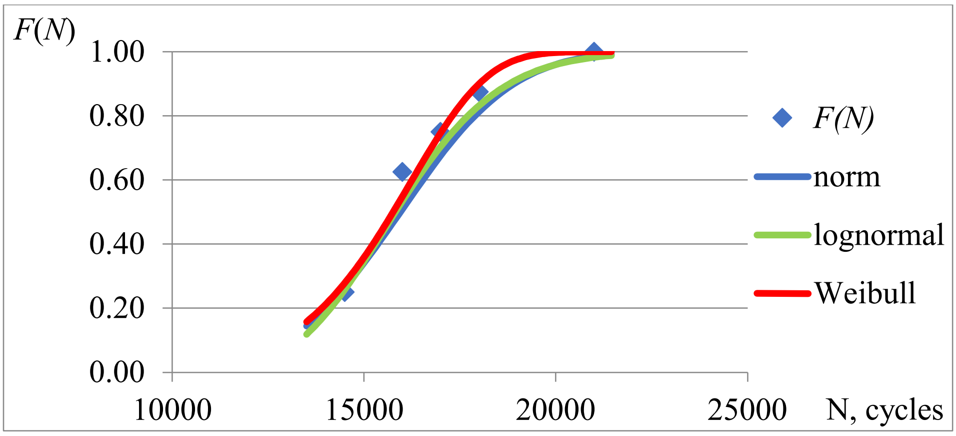

Fig. 2.8. The cumulative probability function approximation for group 5-IV, a = 7 mm.

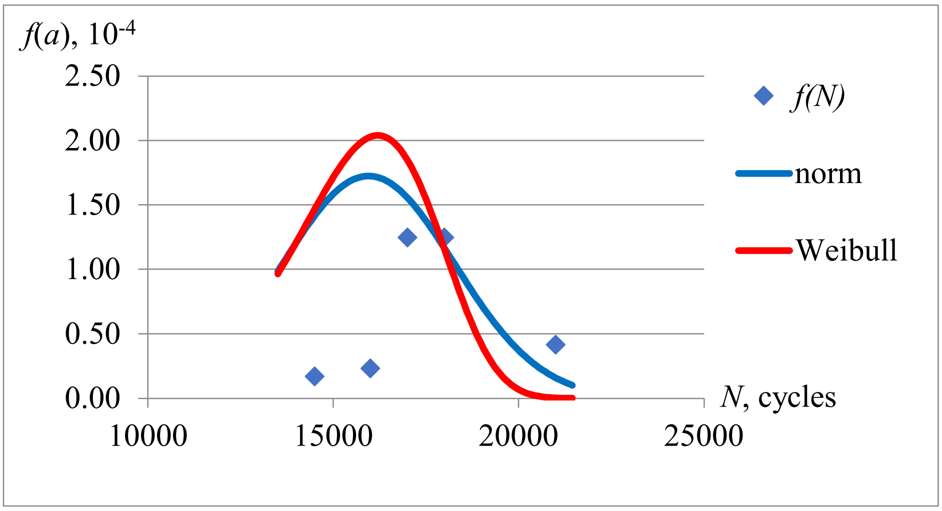

Fig. 2.9. The probability density function approximation for group 5-IV, $a = 7$ mm.

From this data it is obvious that the assumption about relevance of Weibull distribution for fatigue data analysis is correct for this case. Moreover, in each case the R^2 coefficient during the procedure of Weibull's parameters determination is rather high. This fact proves that the Weibull distribution is close to the real data distribution. The Weibull parameters for each approximation and the R^2 coefficient are given in table 2.5.

Table 2.5.

Weibull approximation data for test group 5-IV

Crack size, mm	R^2	Weibull parameters	
		α	β
7	0.989	9.034	16499
10	0.952	9.670	32208
15	0.965	9.370	48950

Therefore, with the increase of crack size the approximation slightly weakens (but still is adequate). Weibull shape parameter β tends to increase logarithmically, as shown on fig. 2.10.

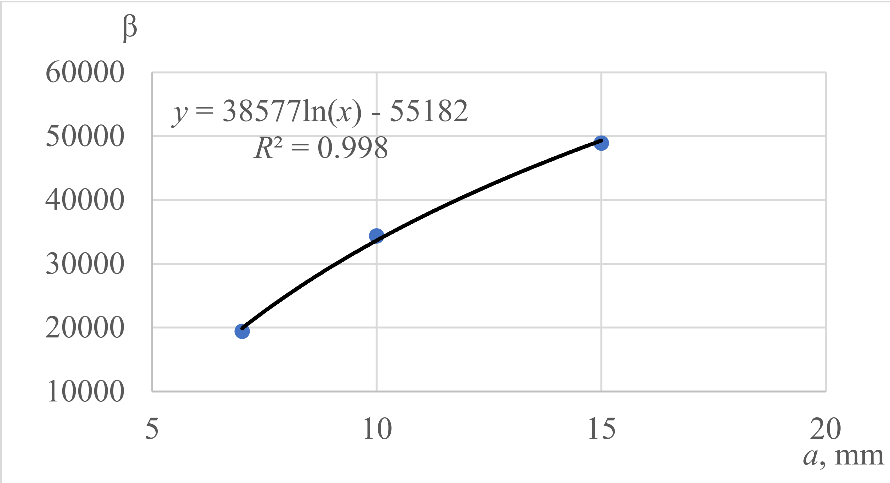

Fig. 2.10. Shape parameter β for Weibull distribution of group 5-IV.

The mentioned shape parameter is proportional to mean number of cycles to reach such crack length, therefore this proves that Weibull approximation was performed correctly, as it is well-known (and proved above) that function $N(a)$ has logarithmic nature.

The distributions of cycles on same crack lengths for group 5-II were found and are given in Appendix D, fig. D.5-D.10.

From the results of these approximations, such conclusions may be made. Again, it is obvious that Weibull distribution is highly accurate, proven by high R^2 in the Weibull parameters determination, which coincides with the theory. Therefore, Weibull distribution will be considered the most suitable furthermore. Weibull distribution parameters and R^2 coefficient is shown in the table 2.6.

Table 2.6

Weibull approximation data for test group 5-II

Crack size, mm	R^2	Weibull parameters	
		α	β
7	0.995	9.67	19477
10	0.990	18.34	34411
15	0.93	28.24	48927

Again, the correlation coefficient drops with the increase of cycles number, this time even more drastically. However, it is possible that there is some issue with the crack size of 15 mm, as it seems that the R^2 value drops too much compared to the tendencies discovered before. It is possible that it is a case of random deflection as the sample size is still rather small and the influence of individual tests randomness is not completely eliminated. Yes, it is possible that some large internal defect or residual stresses were present in some of the samples or the test procedures were violated without reporting that changed the results closer to larger cracks. The tendency to Weibull parameter β logarithmically increasing, however, is found in this data again, as shown in fig. 2.11. This proves that previous approximation is adequate.

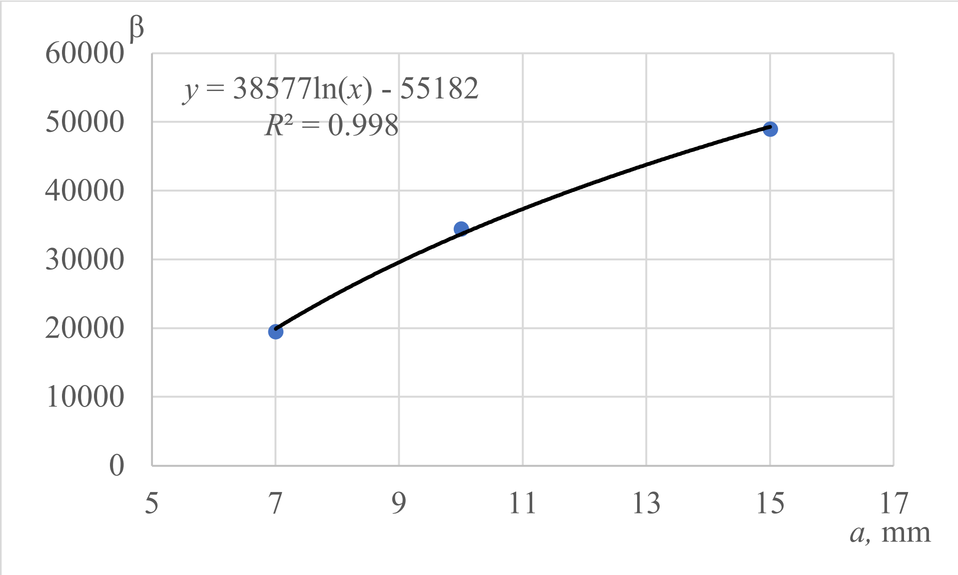

Fig. 2.11. Shape parameter β for Weibull distribution of group 5-II.

2.3.2.2. Intergenerational results comparison

To study the effect of the influence of generations on the statistical analysis results, the data will be represented for both generations on each crack length level. Only Weibull distributions are taken into account during this analysis as it has been proven that such distribution describes fatigue processes the best. The typical graph for such comparison is given on fig. 2.12., and the other graphs may be found in Appendix E, fig. E.1-E.2.

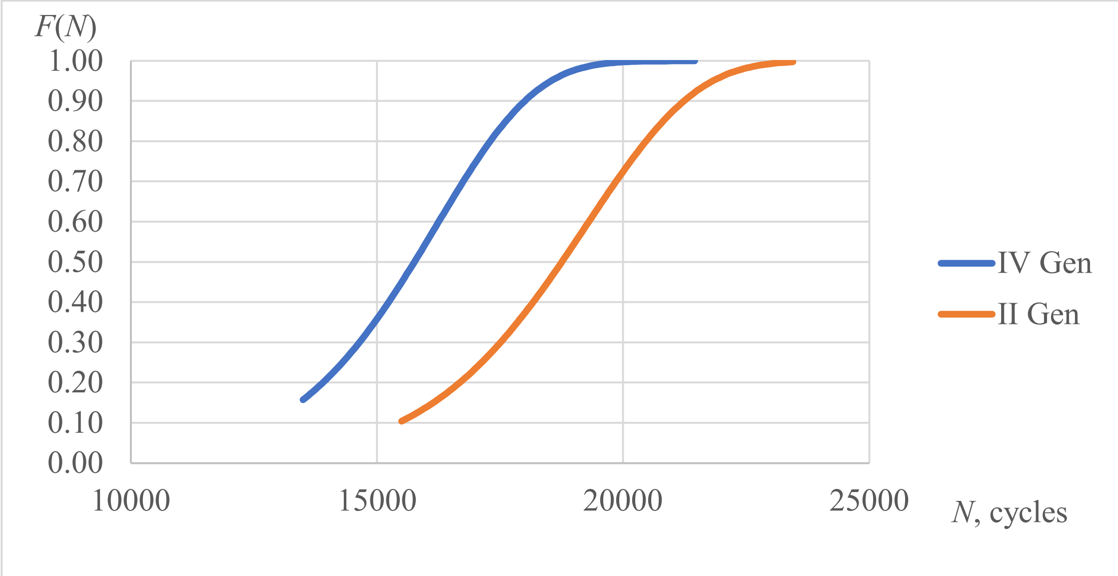

Fig. 2.12. Weibull distribution for a = 7 mm comparison.

Here, an interesting result may be observed. At first, it is always more likely for the crack to grow to 7 mm at less cycles number for larger generation. However, with the crack growth, this effect seems to decrease, as cycles with high the likelihood of appearance of 10 mm crack is rather close for both generations, and for crack of 15 mm length it seems that the likelihood of its appearance becomes even larger from around 48000 cycles for generation II. However, it is advisable to remember about the weak correlation of data for a = 15 mm for group 5-II, the possible reasons of which were discussed earlier. It is rather possible that it influenced the results – but the scope of its suspected influence on generational effects and its impact will be discussed further.

Finally, from the table 2.5 and table 2.6 it is seen that the correlation of Weibull distribution is generally slightly stronger for generation II (except for discussed 15 mm level). This is in line with previous observations of increased randomness for generation IV.

2.3.3. Analysis of cracks lengths probabilities on set number of cycles

2.3.3.1. Comparison on same generation

By the described above procedure, cumulative probability functions and probability density functions were approximated for three levels of cycles. The levels were chosen to be 1000 cycles, 20000 cycles and 40000 cycles. Such choice is to get data on various cycles levels. The graphs of typical approximation result are shown on fig. 2.13-2.14. The graphs of all other results for group 5-IV may be found in Appendix F, fig. F.1-F.4.

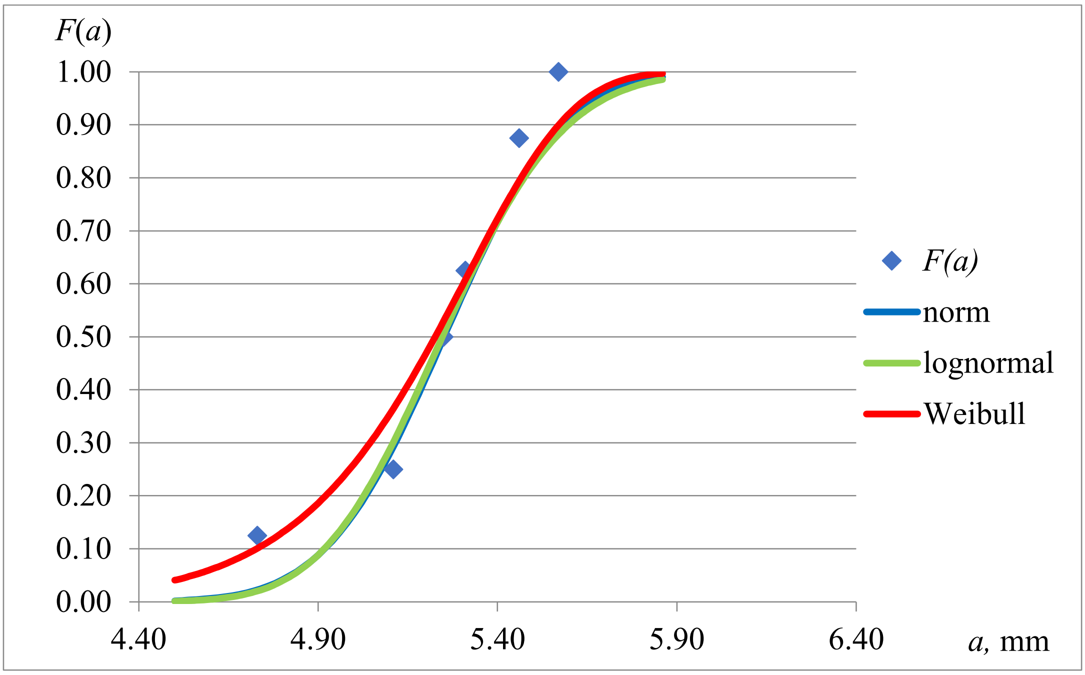

Fig. 2.13. The cumulative probability function approximation for group 5-IV, $N = 1000$ cycles.

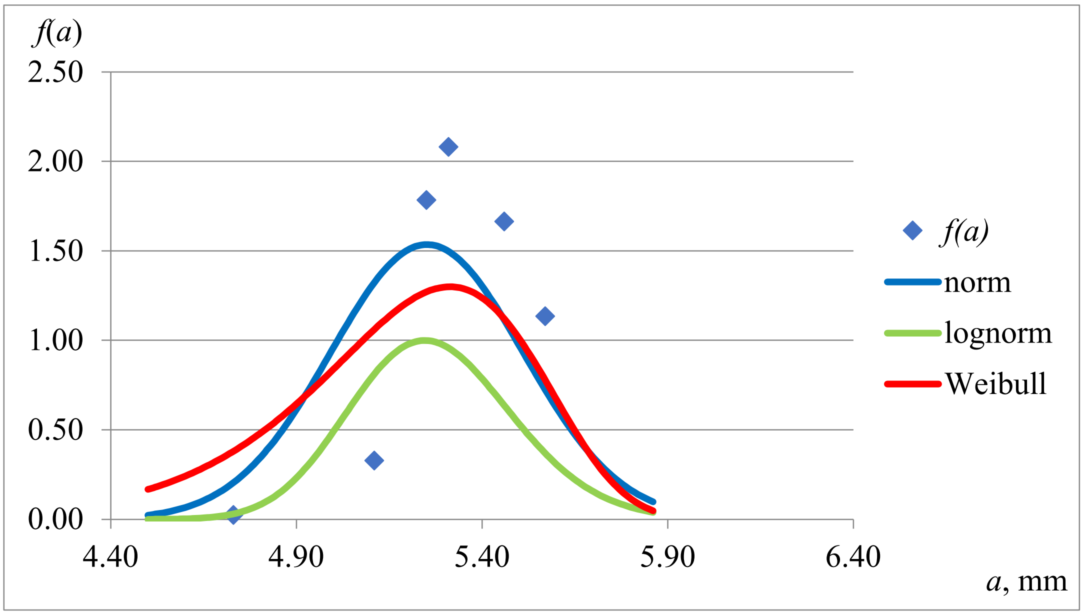

Fig. 2.14. The probability density function approximation for group 5-IV, $N = 1000$ cycles.

Based on the results, it is again obvious that Weibull distribution describes the process in the best way. However, for such results the correlation tends to be weaker than for approximation of $F(N)$, as proven by the values of R^2, shown in table 2.7.

Table 2.7

The Weibull approximation data for test group 5-IV

Cycles number	R^2	Weibull parameters	
		α	β
1000	0.9446	18.805	5.33
20000	0.9214	17.933	7.83
40000	0.968	7.337	12.99

It seems that this time there is no dependance between correlation strength and cycles number – it is weaker in all cases, but strong enough for Weibull distribution to be applicable. Parameter α does not show any dependencies, however, parameter β this time grows exponentially, as shown on fig. 2.15. Such growth shows that Weibull distribution approximation was performed correctly, as parameter β in this case is proportional to the mean crack length at according cycles number, and it is well-known (and proven earlier) that crack length should grow exponentially with time.

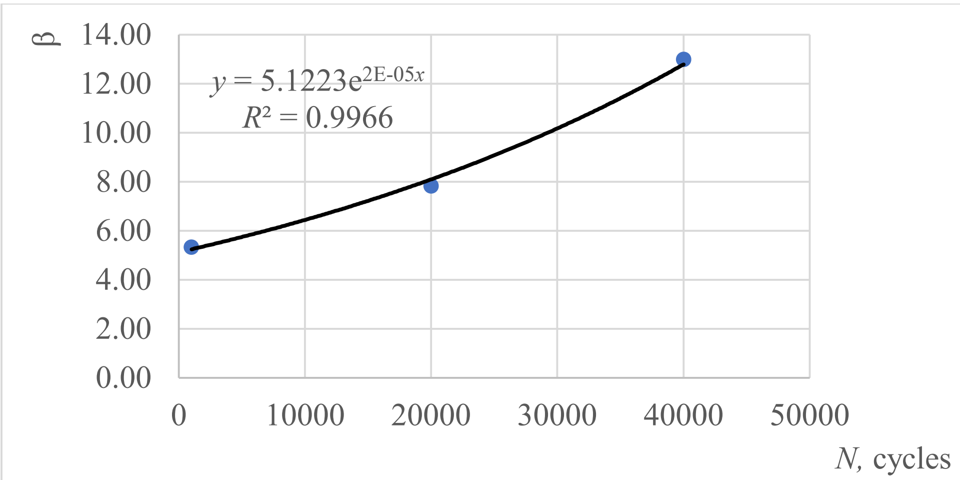

Fig. 2.15. Shape parameter β for Weibull distribution of group 5-IV.

The distributions for group 5-II were found and are given in Appendix F, fig. F.5-F.10.

Again, it is obvious that Weibull distribution describes the results in the best way, as in all previous cases. Interestingly enough, this time approximation, while still weaker than that one of $F(a)$, is rather strong, as proven by the R^2 coefficient given in table 2.8.

Table 2.8

Weibull approximation data for test group 5-IV

Cycles number	R^2	Weibull parameters	
		α	β
1000	0.976	17.56	5.04
20000	0.9959	16.18	7.39
40000	0.9855	18.82	12.31

Similarly to the previous result, R^2 coefficient is not dependent on cycles number here. Moreover, there is no drop of it for larger cycles numbers as during the approximation for $F(N)$. However, it is explained by the fact that the data inconsistency happened closer to approximately 48000 cycles and its' influence is not so strong in this data set. Finally, Weibull parameter β exponentially grows again, proving that the Weibull approximation was performed adequately.

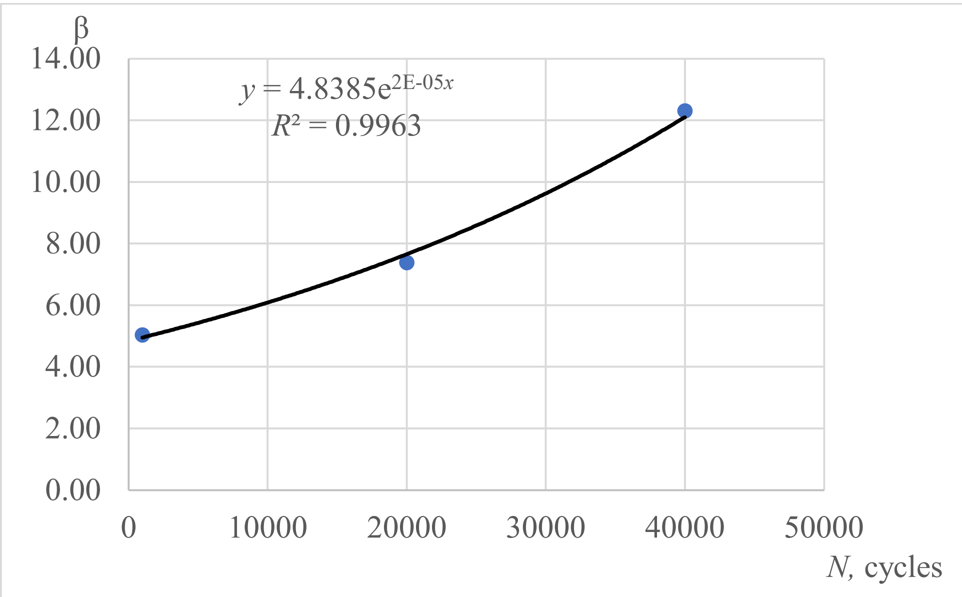

Fig. 2.16. Shape parameter β for Weibull distribution of group 5-II.

2.3.3.2. Intergenerational results comparison

To compare the results approximation for different generations, the approximation data for each cycles level were compiled on same graph. The typical graph for such comparison is given on fig. 2.17, and the other graphs may be found in Appendix G, fig. G.1-G.2.

As Weibull distribution was determined to be the most applicable for this case, only the results of Weibull approximation will be shown.

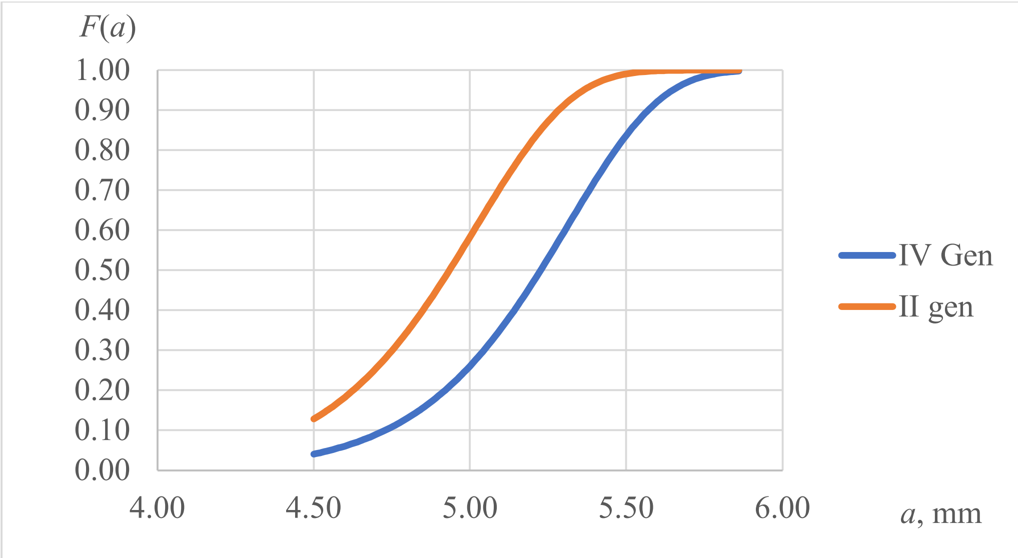

Fig. 2.17. The probability of less than *a* mm crack appearance on $N = 1000$ cycles.

Therefore, it seems that it is practically always more probable to meet longer cracks on the sample of larger generation on same number of cycles. The tendency is a little disrupted for N = 40000, what may be explained by the mentioned above problems that seem to accumulate with time closer to 48000 cycles. More detailed discussion of the generational differences and their possible reasons will be presented in 2.3.4.

Also, it is important to notice that in this case R^2 coefficients during Weibull distribution determination procedure tend to be much higher for the tests of group 5-IV. This further proves the observation of increased randomness in "older" generations.

2.3.4. The study of generational effect on the tests results

As it was discussed before, the samples for the tests were manufactured from the samples that had already been broken as a result of previous tests of crack growth and residual strength. During the experiment it has been assumed that the generational effect influence will be, if any, rather weak as the most stress intensity will happen near the tip of the pre-made slot and pre-grown crack. While this is true in terms that the crack and latter static destruction in residual stress tests will definitely grow from the place with the most stress intensity, which is obviously the slotted part (guaranteed at least mediocre quality of manufacturing), it does not mean that minor plastic deformations throughout the rest of material are completely out of the picture. It is likely that during previous tests some plastic deformations and slips do happen in the places of higher stress intensity due to natural non-homogeneity of material. Such defects may, in fact, reduce the endurance in the next test if they are located along the way of the crack growth. However, it is likely that such deviances will have even more random character as they depend on chance of such defects being in the part of material new sample is made of and simultaneously happening along the crack length. As such internal defects are, of course, very numerous, in general they will influence each test to some degree, however, the variance of the influence will be greater with generations.

To check this assumption, such procedure has been applied. Firstly, the test results of series of interest were grouped according to their cycles number (for example, all samples' crack lengths at 1000 cycles, 5000 cycles and so on). Then, average of each group was found. Then, the results were approximated using MS Excel according to the exponential law:

$$a = \alpha e^{\beta N},$$

where a – average crack length of all samples of this series on N cycles, α and β – coefficients. After that, the expressions were divided to get coefficient k_{gen} and the tendency of its change with cycle number growth.

For the tests of groups 5-IV and 5-II the coefficient is:

$$k_{gen} = \frac{a_{IV}}{a_{II}} = \frac{4.923e^{2.31\cdot10^{-5}}}{4.674e^{2.24\cdot10^{-5}}} = 1.053e^{6.2\cdot10^{-7}}.$$

Fig. 2.18 shows the dependance of k_{gen} on cycles number for this case.

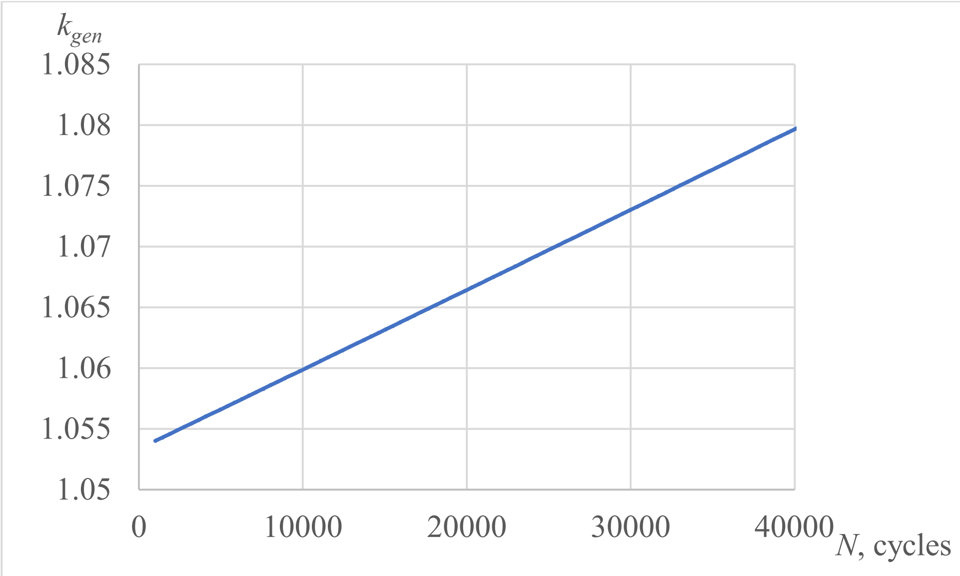

Fig. 2.18. The generational coefficient (groups 5-IV and 5-II).

Note that for this approximation only data up to 40000 cycles was used to eliminate the influence of the mentioned above unnatural processes that begin to show around 40000 cycles.

Therefore, it seems that not only the crack length is always larger at "older" samples, but also the gap in size exponentially (though the exponentiality of the process is so weak that it could be approximated linearly with rather high accuracy) increases with increase in the cycles number. It may be explained by the fact that as the crack growth in size, it encounters more and more mentioned pre-deformed zones and slips that slightly contribute to the process of crack growth – and as the longer the crack, the faster it grows, the crack with a "headstart" continues to accelerate its growth and the difference in size increases.

However, it is an improper practice to base all of the conclusions on only one example. Therefore, the same analysis will be performed on test samples of groups 3 - III and 3 - I. Both results were approximated by the same procedure of averaging and applying the exponential law to the data and dividing the expressions for a to get the law for k_{gen}. The coefficient was determined as:

$$k_{gen} = \frac{a_{III}}{a_I} = \frac{3.783e^{0.00002N}}{3.822e^{0.0000157N}} = 0.9898e^{4.4\cdot10^{-6}N}.$$

Fig. 2.19 shows the dependance of k_{gen} on cycles number for this case.

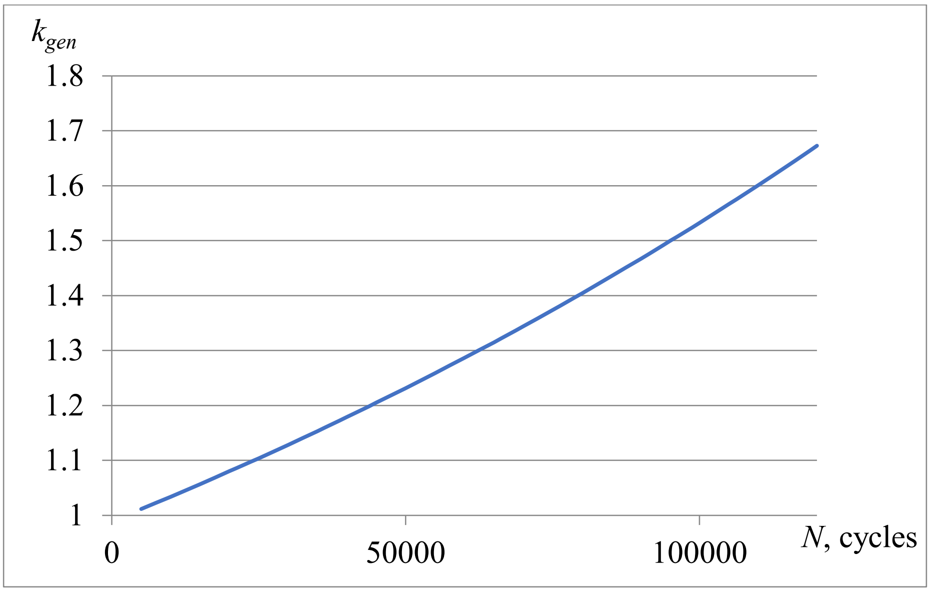

Fig. 2.19. The generational coefficient (groups 3-III and 3-I).

Note that for this approximation data up to 120000 cycles was used as test for these tests lasted longer because the samples themselves were larger. Also note that test group 3-I consisted only of 4 samples, therefore the results of this approximation may be a little less representative.

Again, the trend for exponential growth is seen. It may look that the coefficient grows much shaper, but it is just an illusion caused by much greater range of cycles axis of this graph. While the growth up to 40000 cycles is indeed around twice quicker, this may be explained by the fact that this time one of the compared groups belongs to the I generation, therefore, completely eliminating the effect of randomness that is caused by plastic micro-deformations and slips.

Finally, the groups of 3-III and 3-I will be compared to their group 5-IV and 5-II children. For group 3-I:

$$k_{gen} = \frac{a_{II}}{a_I} = \frac{4.673e^{0.00002245N}}{3.822e^{0.00001566N}} = 1.2228e^{6.8\cdot10^{-6}N}.$$

Fig. 2.20 shows the dependance of k_{gen} on cycles number for this case.

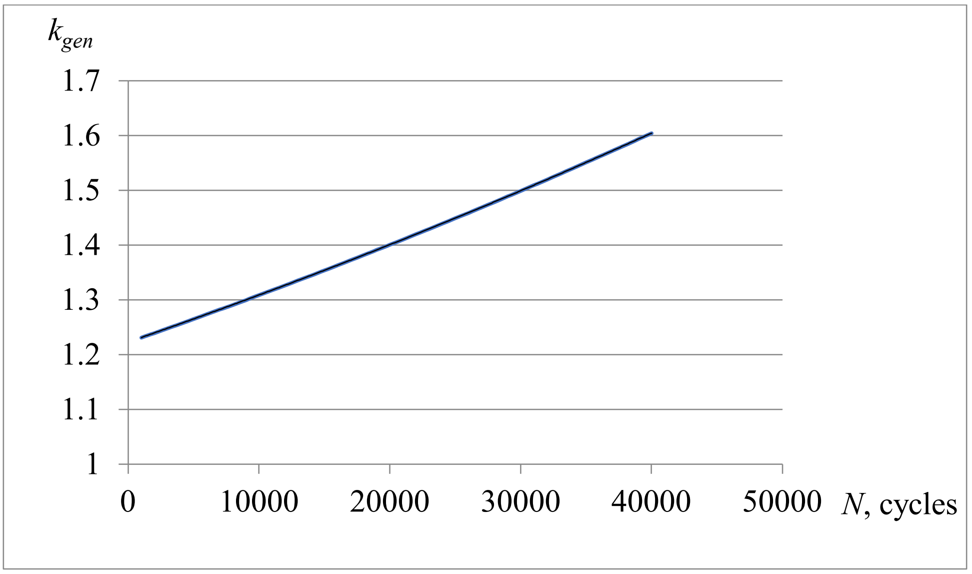

Fig. 2.20. The generational coefficient (groups 3-I and 5-II).

For group 3-III:

$$k_{gen} = \frac{a_{IV}}{a_{III}} = \frac{4.9456e^{0.00002277}}{3.783e^{0.00002}} = 1.3073e^{2.7\cdot10^{-6}N}.$$

Fig. 2.21 shows the dependance of k_{gen} on cycles number for this case.

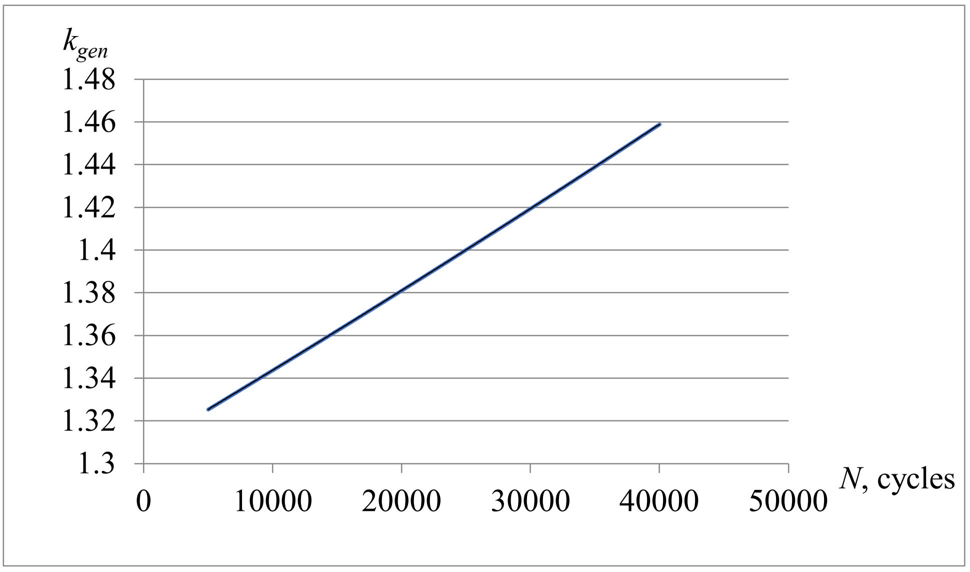

Figure 2.21. The generational coefficient (groups 3-III and 5-IV).

Therefore, it may be seen that the trend of the generational coefficient increase with cycles number continues for those two cases. Moreover, for the groups 3-III and 5-IV the increase is less sharp than that of groups 3-I and 5-II. This proves the assumption about sharper difference when one of the compared samples is new.

It is required to note, however, that the last two coefficients are not purely generational ones as in this case, size of the samples changed too. There is lack of data about the relation between crack growth rates and samples size, therefore, some internal factors may influence the values. Nonetheless, these results are in line with earlier conclusions and can be taken as additional proof of assumption about exponential increase of generational coefficient with cycles number.

2.4. Application of the gained data for fatigue life prediction

2.4.1. The reasons and mathematical basis for application of tests results

As it was mentioned earlier, the 2524 series of aluminum may be used for fatigue-prone zones of the skin and lower wing surface of the designed aircraft. A relevant topic appears than – a problem of providing adequate damage tolerance between maintenances and determining the frequency of said maintenance. To do that, it is possible to apply obtained before results. Yes, by taking the probability density function's definite integral, it is possible to find the probability of event happening between these points. By the Newton-Leibniz formula, the definite integral of Weibull probability density function in general case is found as:

$$\int_a^b f(x)dx = F(b) - F(a). \tag{2.3}$$

The expression for the indefinite integral of Weibull probability density is well-known, and it is its cumulative probability function, stated in formula (2.1).

2.4.2. Set length cracks appearing probability

In practice, it is important to know when it is practically guaranteed for fatigue damage to increase not too fast. For such estimation, 95% parameter is used [7,8]. It is such number of cycles that there is a 95% probability that the crack will not happen before some number of cycles (or in this case, crack will not grow to the given size).

Such value is determinable from the approximation results. To do that, it is required to equate the formula (2.3) to 0.05 (as the probability of crack growth *happening* was determined, 95% chance of crack growth *not happening* correspond to 5% in the function of crack growth *happening*), take the lower integration limit as 0 (as the goal of the calculation is to check whether crack happened *up to* some number). The upper integration N limit therefore will be the number of interest. The procedure is shown below:

$$0.05 = \left(1 - \exp\left[-\left(\frac{N}{\beta}\right)^{\alpha}\right]\right) - \left(1 - \exp\left[-\left(\frac{0}{\beta}\right)^{\alpha}\right]\right) = 1 - \exp\left[-\left(\frac{N}{\beta}\right)^{\alpha}\right];$$

$$0,95 = \exp\left[-\left(\frac{N}{\beta}\right)^{\alpha}\right];$$

$$\ln(0.95) = -\left(\frac{N}{\beta}\right)^{\alpha};$$

$$\beta\sqrt[\alpha]{\ln(\tfrac{1}{0.95})} = N.$$

The results of such calculation for each group and crack length are given in table 2.9.

Table 2.9

Cycle number for cracks to be guaranteed less than *a* mm

Test group	Crack length a, mm	$N_{95\%}$, cycles
5-IV	7	10829
	10	21732
	15	32616
5-II	7	13142
	10	27965
	15	42761

Such analysis allows to provide set periods where it is practically guaranteed that the crack will not happen. Therefore, if allowable limits of crack lengths are developed, the periodical maintenance procedures that check for the existence of such crack should be planned to start after $N_{95\%}$, as it is practically impossible to meet it earlier. The allowable crack lengths limits should be derived based on the practical details of the component role, location and geometry and their derivation is not described in this work. Finally, note that these data values (and ones obtained in further subchapters) represent the number of cycles required for the crack to *grow* from the starting length a_0 used in test. To obtain cycle values that incorporate the process of crack initiation, it is required to combine these results with studies of crack initiation processes.

2.4.3. Probability of the longest crack appearing on set number of cycles

A reverse task may be relevant too – when scheduling maintenance and predicting the life of the aircraft, it is useful to know the largest defect size that may happen on some set values of cycles (as cycles represent real flight procedures) to prevent reaching critical crack before next maintenance. Again, it is appropriate to use the probability of 95%, $a_{95\%}$ - the crack size that it is practically guaranteed to be the largest crack possible to be found on such cycle numbers. Determination of such crack size was performed by the same procedure as one described in 2.4.2, however, this time the probability of interest is indeed 95%, as it is required to determine the crack length that is guaranteed to be *the largest* crack expected:

$$0.95=\left(1-\exp\left[-\left(\frac{N}{\beta}\right)^{\alpha}\right]\right)-\left(1-\exp\left[-\left(\frac{0}{\beta}\right)^{\alpha}\right]\right)=1-\exp\left[-\left(\frac{N}{\beta}\right)^{\alpha}\right];$$

$$0,05=\exp\left[\left(-\frac{N}{\beta}\right)^{\alpha}\right];$$

$$\ln(0.05)=-\left(\frac{N}{\beta}\right)^{\alpha};$$

$$\beta\sqrt[\alpha]{\ln(\tfrac{1}{0.05})}=N.$$

The results of such calculation for each group and cycles number are given in table 2.9.

Table 2.9.

The cracks size that is guaranteed to be largest on *N* cycles

Test group	Cycles number	$a_{95\%}$, mm
5-IV	1000	5.40
	20000	7.95
	40000	13.5
5-II	1000	5.12
	20000	7.51
	40000	12.48

2.4.4. Prediction of generational influence on crack size

When a fatigue crack is found in service on the fuselage skin panels, usually the skin panel is not replaced completely. A repair is made to cover the cracked part by a patch of new metal by either riveting or bonding to carry part of the loads [12]. However, while it is true that largely the crack grew from place (places, often there exist a case of multiple cracks presence on one element) where the stress intensity was the largest, it has been proven by the analysis of experimental data above that it is not entirely correct to consider that the rest of material is truly unaffected. Therefore, the post-maintenance state of the part would be actually closer to the state of the samples of "older" generation, as some internal deformations and slips will be present. So in practice it is important to know how much earlier it is required to conduct testing for cracks on pre-maintenanced components, which may be determined by the results of tests.

For example, let a crack grew to the critical size on a new skin panel and was repaired. Then a new crack grew on the same panel and was repaired again. Now the task is to determine when another crack would grow to the critical size. Let the critical size be 20 mm, as described in source [8] and it happened at first generation on 102000 cycles. Then it is possible to use the k_{gen} obtained in comparison of results of comparison of groups 3-III and 3-I to predict the decrease in cycles number. Coefficient k_{gen} is determined in such way:

$$k_{gen} = \frac{a_{III}}{a_I} = 0.9898 e^{4.4 \cdot 10^{-6} N}.$$

It is known that a_{III} = 20 mm and N = 102000. Therefore, the equivalent crack of third generation on the same cycles number on first generation a_I would be found as:

$$a_I = \frac{a_{III}}{k_{gen}} = \frac{20}{0.9898 e^{4.4 \cdot 10^{-6} \cdot 102000}} = 12.9 \text{ mm}.$$

From the observations of crack growth of first generation, it is possible to find when such crack size happened. In the example used the data from average approximation of group 3-I was used, and by it such number of cycles would be N = 63000 cycles. In such case it would be expected to find critical crack twice faster!

However, it is important to note that while results in earlier predictions based on rather representative data samples, this prediction is shown just as a proof of concept as it based on the averaging of results of only one experiment group and is not backed by any earlier researches. Therefore, it is recommended to provide more thorough experiments with the purpose of study of generational effect and correlation of such data with reality to be able to apply these results for real engineering problems.

Conclusions to the special part

In conclusion, the study of dependencies of crack growth processes in the aluminum alloy 2425 used on for the fuselage skin and lower wing panels for the designed aircraft is one of the most important stages of design process as it is required to provide safety in operation of the structure. The calculations performed were aimed to assess the materials properties to provide possibility of creation of damage tolerant structure for fuselage skin and lower wing panels. Moreover, the generational effect was studied on the samples that were already loaded before.

The results of the calculation shown that the crack growth processes may be accurately enough predicted by Weibull distribution. Furthermore, it has been shown that it is improper to assume that there is no generational influence on the pre-loaded samples.

.

GENERAL CONCLUSIONS

1. A preliminary design of a heavy cargo aircraft with 200000 kg payload was completed in this project according to the task. All main dimensions and location of all principal units were determined based on purpose, designed payload, flight parameters, take-off and landing conditions. The design meets the general requirements for cargo aircraft. Layout planning and analysis of the cabin was made according to the task and centering was carried out. The location of the center of mass is determined to be inside of the accepted statistical tendencies. Drawings of the aircraft were made based on the An-124 prototype.
2. The crack growth processes in the tests are behaving according to the Weibull distribution and are approximated by it with high accuracy, proven by high R^2 coefficients during its coefficient's determination and correct tendencies of β parameter dynamics.
3. Based on the determined cumulative probability functions approximated by Weibull distribution, it is possible to determine the probability of crack growth to specific size with various cycles numbers, and the probability of cracks of various sizes growth after specific cycles number passing. “Guaranteed” values that define the time for scheduled maintenance can be calculated.
4. It is not correct to assume that cyclic loading affects only zones with highest stress intensity, as the samples made of the previous samples' leftovers show different characteristics due to the generation of plastic microdeformations and slips during previous loading. Therefore, any tests that seek to determine the pure characteristics of material should be performed on new samples only.
5. The “older” samples are practically always expected to have longer cracks on same cycles number and need significantly less cycles to reach cracks of the same length compared with new samples and samples of previous generations.

6. The influence of the generations on crack length difference is increasing exponentially with the increase of cycle number.
7. The influence of generational effect increases with cycles in sharper manner when comparing with the new samples due to complete absence of plastic microdeformations in them, but the tendency of its exponential increase is found in all generations' comparison.
8. Generally, all results gathered from the samples of older generations are showing more randomness during most of analysis, proved by the smaller R^2 coefficient and visually observed scattering on diagrams due to randomly distributed microdeformations and slips from previous loadings.

REFERENCE

1. Конструкція та міцність літальних апаратів: методичні рекомендації до виконання курсового проєкту для студентів спеціальності 134 «Авіаційна та ракетно-космічна техніка» /уклад. С.Р. Ігнатович, М.В. Карускевич, Т.П. Маслак, С.В. Хижняк, С.С. Юцкевич – К.: НАУ, 2018.

2. Goodyear aviation databook. Global Aviation Tires, The Goodyear Tire & Rubber Company, 2016.

3. Megson T. H. G. Aircraft Structures for engineering students. Third Edition. MPG Books Ltd, 1999.

4. Rowan Healey, John Wang, Wing Kong Chiu, Nabil M. Chowdhury, Alan Baker, Chris Wallbrink. A review on aircraft spectra simplification techniques for composite structures, Composites Part C: Open Access, Volume 5, 2021, 100131, ISSN 2666-6820, https://doi.org/10.1016/j.jcomc.2021.100131.

5. Roberta Lazzeri. A COMPARISON BETWEEN SAFE LIFE, DAMAGE TOLERANCE AND PROBABILISTIC APPROACHES TO AIRCRAFT STRUCTURE FATIGUE DESIGN. L'Aerotecnica, Missili e Spazio. 2. – 2002

6. Discussion of the Differences Between Fail-Safe and Damage Tolerant Philosophies. Preamble, FAR Amendment 25-72. https://www.faa.gov/sites/faa.gov/files/FS_vs_DTl.pdf.

7. Ulf G. Goranson. Fatigue issues in aircraft maintenance and repairs. nt. Fatigue Vol. 20, No. 6, pp. 413–431, 1997. The Boeing Company. Published by Elsevier Science Ltd. Printed in Great Britain.

8. UIf G. Goranson. Elements of structural integrity assurance. Fatigue Vol. 16, No. 1, 1994. Butterworth-Heinemann Ltd.

9. Aluminum Standards and Data 2000. Aluminum Association, 2013.

10. Maduro, L & Baptista, C. & Torres, S & Souza, Renato. Modeling the growth of LT and TL-oriented fatigue cracks in longitudinally and transversely

pre-strained Al 2524-T3 alloy-review under responsibility of ICM11. Procedia Engineering. 10. 1214-1219, 2011

11. ASTM E647-15e1. Standard Test Method for Measurement of Fatigue Crack Growth Rates.

12. Robert S. Fredell. Damage Tolerant Repair Techniques for Pressurized Aircraft Fuselages, 1994.

Appendix

APPENDIX A. INITIAL DATA

Passenger Number	0.
Flight Crew Number	4.
Flight Attendant or Load Master Number	4.
Mass of Operational Items	2617.37 kg
Payload Mass	200000.00 kg
Cruising Speed	860 km/h
Cruising Mach Number	0.7846
Design Altitude	9.00 km
Flight Range with Maximum Payload	4000.00 km
Runway Length for the Base Aerodrome	3.30 km
Engine Number	4.
Thrust-to-weight Ratio in N/kg	2.3200
Pressure Ratio	40.00
Assumed Bypass Ratio	6.50
Optimal Bypass Ratio	5.50
Fuel-to-weight Ratio	0.2400
Aspect Ratio	8.60
Taper Ratio	3.04
Mean Thickness Ratio	0.120
Wing Sweepback at Quarter Chord	29.0 deg
High-lift Device Coefficient	1.100
Relative Area of Wing Extensions	0.000

Wing Airfoil Type – supercritical
Winglets – not used
Spoilers – used

Fuselage Diameter	8.40 m
Finess Ratio	10.00
Horizontal Tail Sweep Angle	32.0 deg
Vertical Tail Sweep Angle	38.0 deg

CALCULATION RESULTS

Optimal Lift Coefficient in the Design Cruising Flight Point	C_y	0.40405
Induce Drag Coefficient	$C_{x.ind}$	0.00916

ESTIMATION OF THE COEFFICIENT $D_m = M_{critical} - M_{cruise}$

Cruising Mach Number	M_{cruise}	0.78462
Wave Drag Mach Number	$M_{critical}$	0.80015
Calculated Parameter D_m	D_m	0.01553

Wing Loading in kPa (for Gross Wing Area):

At Takeoff	6.099
At Middle of Cruising Flight	5.380

At the Beginning of Cruising Flight	5.912
Drag Coefficient of the Fuselage and Nacelles	0.00766
Drag Coefficient of the Wing and Tail Unit	0.0091

Drag Coefficient of the Airplane:	
At the Beginning of Cruising Flight	0.02803
At Middle of Cruising Flight	0.02712
Mean Lift Coefficient for the Ceiling Flight	0.40405
Mean Lift-to-drag Ratio	14.89749
Landing Lift Coefficient	1.637
Landing Lift Coefficient (at Stall Speed)	2.456
Takeoff Lift Coefficient (at Stall Speed)	2.014
Lift-off Lift Coefficient	1.470
Thrust-to-weight Ratio at the Beginning of Cruising Flight	0.632
Start Thrust-to-weight Ratio for Cruising Flight	2.198
Start Thrust-to-weight Ratio for Safe Takeoff	2.176

Design Thrust-to-weight Ratio	R_O	2.286
Ratio $D_r = R_{cruise} / R_{takeoff}$	D_r	1.010

SPECIFIC FUEL CONSUMPTIONS (in kg/kN*h):

Takeoff	32.2265
Cruising Flight	57.3836
Mean cruising for Given Range	59.1324

FUEL WEIGHT FRACTIONS:

Fuel Reserve	0.03572
Block Fuel	0.19794

WEIGHT FRACTIONS FOR PRINCIPAL ITEMS:

Wing	0.10319
Horizontal Tail	0.00925
Vertical Tail	0.00920
Landing Gear	0.04460
Power Plant	0.08450
Fuselage	0.08735
Equipment and Flight Control	0.10390
Additional Equipment	0.00453
Operational Items	0.00413
Fuel	0.23366
Payload	0.31579

Airplane Takeoff Weight	"M_o" = 633326 kg
Takeoff Thrust Required of the Engine	361.98 kN

Air Conditioning and Anti-icing Equipment Weight Fraction	
Passenger Equipment Weight Fraction	0.0093
(or Cargo Cabin Equipment)	0.0001
Interior Panels and Thermal/Acoustic Blanketing Weight Fraction	0.0041
Furnishing Equipment Weight Fraction	0.0714

Flight Control Weight Fraction	0.0024
Hydraulic System Weight Fraction	0.0081
Electrical Equipment Weight Fraction	0.0029
Radar Weight Fraction	0.0010
Navigation Equipment Weight Fraction	0.0015
Radio Communication Equipment Weight Fraction	0.0008
Instrument Equipment Weight Fraction	0.0018
Fuel System Weight Fraction	0.0082

Additional Equipment:

Equipment for Container Loading	0.0000
No typical Equipment Weight Fraction (Build-in Test Equipment for Fault Diagnosis, Additional Equipment of Passenger Cabin)	0.0045

TAKEOFF DISTANCE PARAMETERS

Airplane Lift-off Speed	294.14 km/h
Acceleration during Takeoff Run	1.51 m/s^2
Airplane Takeoff Run Distance	2188.00 m
Airborne Takeoff Distance	472.00 m
Takeoff Distance	2660.00 m

CONTINUED TAKEOFF DISTANCE PARAMETERS

Decision Speed	263.82 km/h
Mean Acceleration for Continued Takeoff on Wet Runway	0.47 m/s^2
Takeoff Run Distance for Continued Takeoff on Wet Runway	3023.70 m
Continued Takeoff Distance	3495.94 m
Runway Length Required for Rejected Takeoff	3628.85 m

LANDING DISTANCE PARAMETERS

Airplane Maximum Landing Weight	534312.00 kg
Time for Descent from Flight Level till Aerodrome Traffic Circuit Flight	18.10 min
Descent Distance	43.35 km
Approach Speed	274.38 km/h
Mean Vertical Speed	2.17 m/s
Airborne Landing Distance	526.00 m
Landing Speed	259.38 km/h
Landing run distance	898.00 m
Landing Distance	1424.00 m
Runway Length Required for Regular Aerodrome	2379.00 m
Runway Length Required for Alternate Aerodrome	2023.00 m

ECONOMICAL EFFICIENCY

Maximum Take Off Weight to Payload	1.4127
Empty Loaded Aircraft Weight per Passenger	0
Relative Full-Load Performance of the Aircraft	472.53 kg/passenger
Average Burn of fuel per hour	25318.867 kg/h
Average Burn of fuel per kilometer	31.34 kg/km
Average burn of 1000 kg of fuel per 1km	156.697 g/(t*km)
Average burn of 1000 kg of fuel per 1km per 1 passenger	0
Costs per gross-tone-kilometer	0.1772 $(t*km)

NAU 24 03S 00 00 00 71 EN

#	Object name
1	Wing structure
2	Fuel system
3	Control system
4	Electrical equipment
5	Anti-icing system
6	Hydraulic system
7	Power plant
8	Nose LG
9	Main LG
10	Fuel for flight
11	Reserve fuel

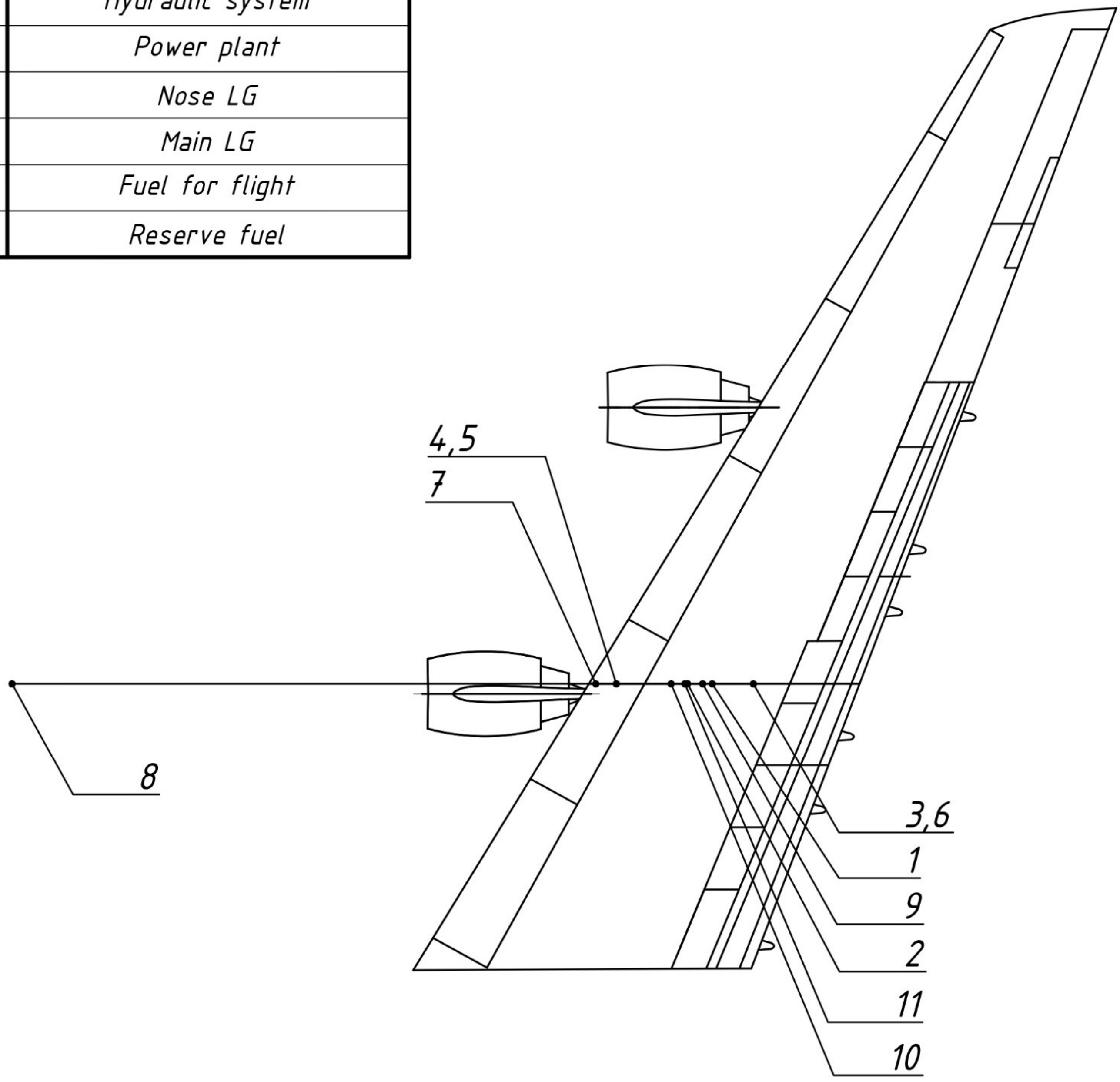

					NAU 24 03S 00 00 00 71 EN			
Ch.	Sh.	Docum. No.	Sign	Date	Equipped wing sketch	Letter	Mass	Scale
Performed		Solin D.				Q		1:300
Supervisor		Krasnopolskyi V.						
Tech. control						Sheet 72		Sheets 85
St. controler		Krasnopolskyi V.			Appendix B	404 ASF 134		
Approved		Yutskevich S.						

NAU 24 03S 00 00 00 71 EN

#	Object name
1	Fuselage structure
2	Horizontal tail unit
3	Vertical tail unit
4	Radiolocation equipment
5	Dashboard and instrument equipment
6	Aeronavigation equipment
7	Radio equipment
8	Control system
9	Electrical system
10	Hydraulic system
11	Anti-icing system
12	Air conditioning system
13	Emergency equipment
14	Tools
15	Water and liquid
16-17	Lavatory
18-19	Galley
20	Cargo loading equipment
21	Interior panels, lining and insulation
22	Pilot's seats
23	Load master's seats
24	Non-typical equipment
25	On board meal
26	Load masters
27	Crew
28	Cargo

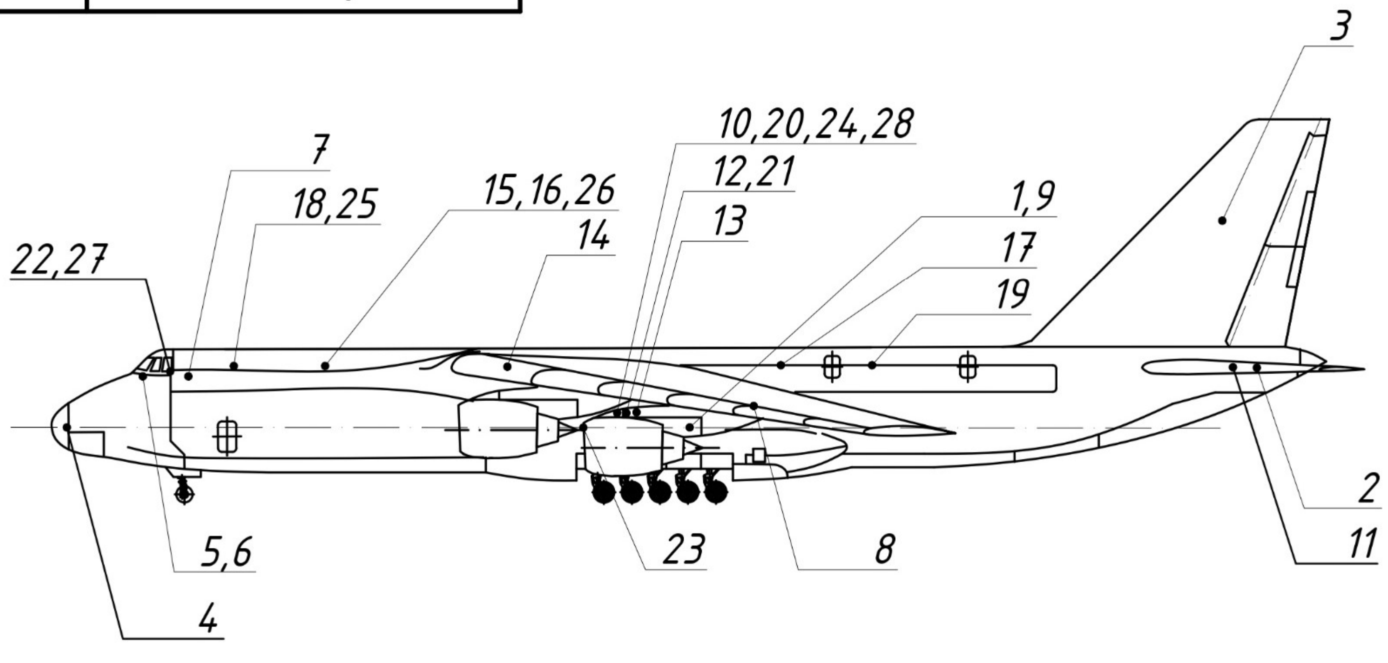

Ch.	Sh.	Docum. No.	Sign	Date	NAU 24 03S 00 00 00 71 EN
Performed		Solin D.			Equipped wing sketch
Supervisor		Krasnopolskyi V.			Letter: Q; Mass; Scale: 1:500
Tech. control					Sheet 73; Sheets 85
St. controler		Krasnopolskyi V.			Appendix B
Approved		Yutskevich S.			404 ASF 134

APPENDIX C. SCHEME OF EQUIPPED FUSELAGEAPPENDIX D. PROBABILISTIC GRAPHS FOR SET LENGTH

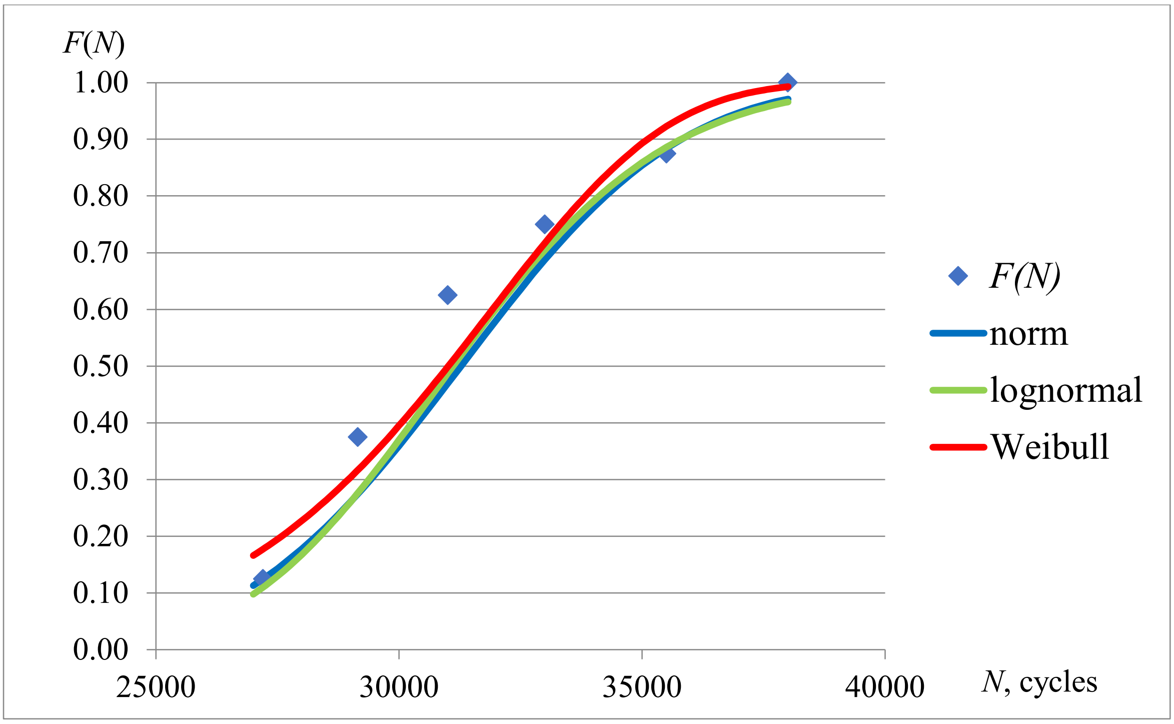

Fig. D.1. The cumulative probability function approximation for group 5-IV, a = 10 mm.

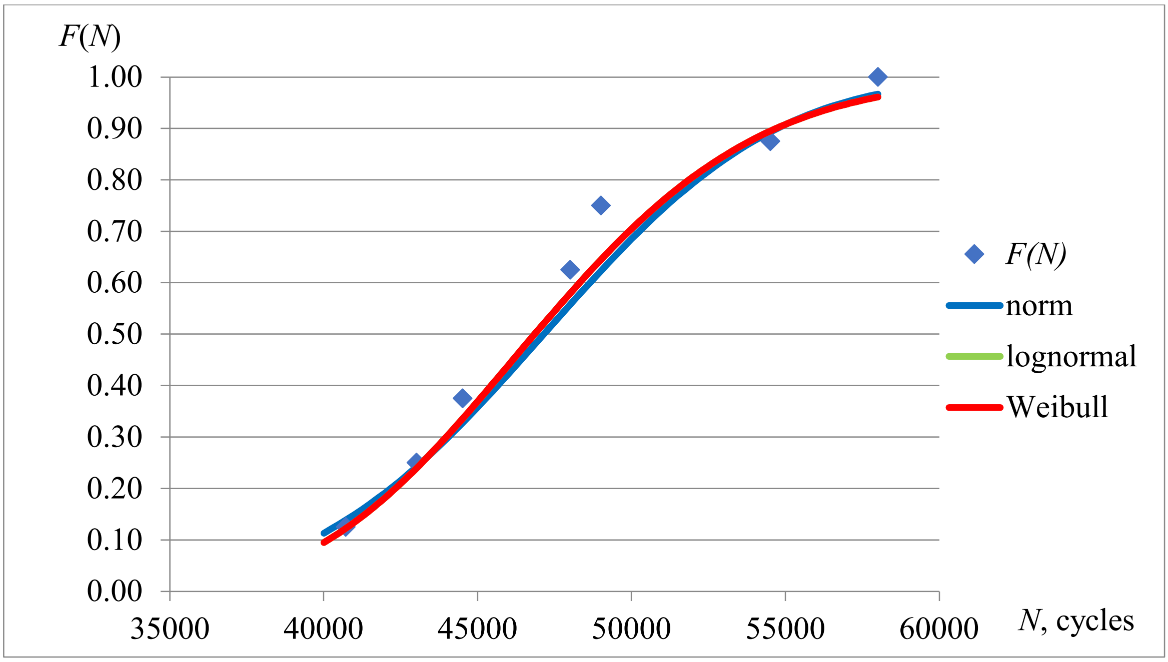

Fig. D.2. The cumulative probability function approximation for group 5-IV, a = 15 mm.

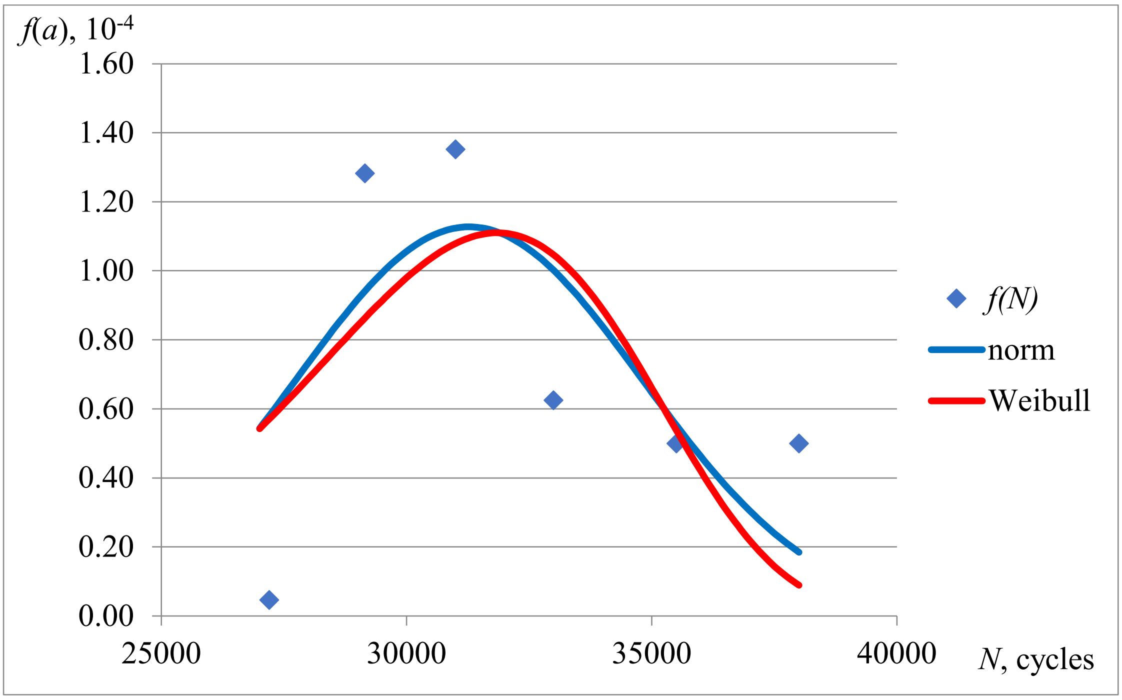

Fig. D.3. The probability density function approximation for group 5-IV, a = 10 mm.

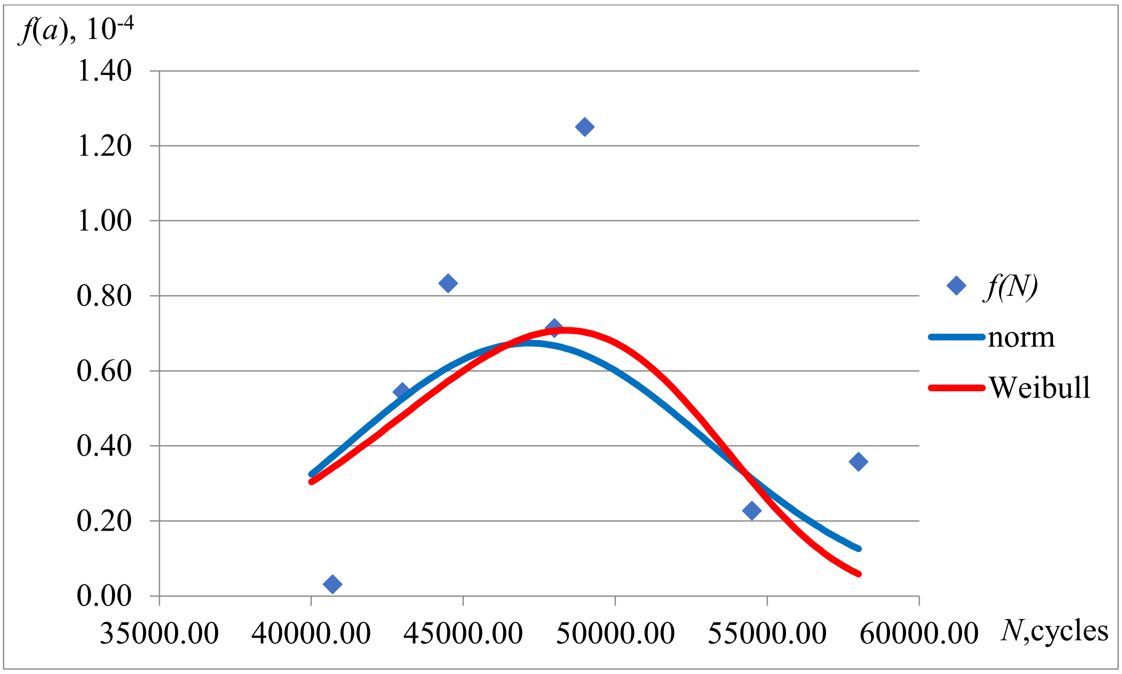

Fig. D.4. The probability density function approximation for group 5-IV, a = 15 mm.

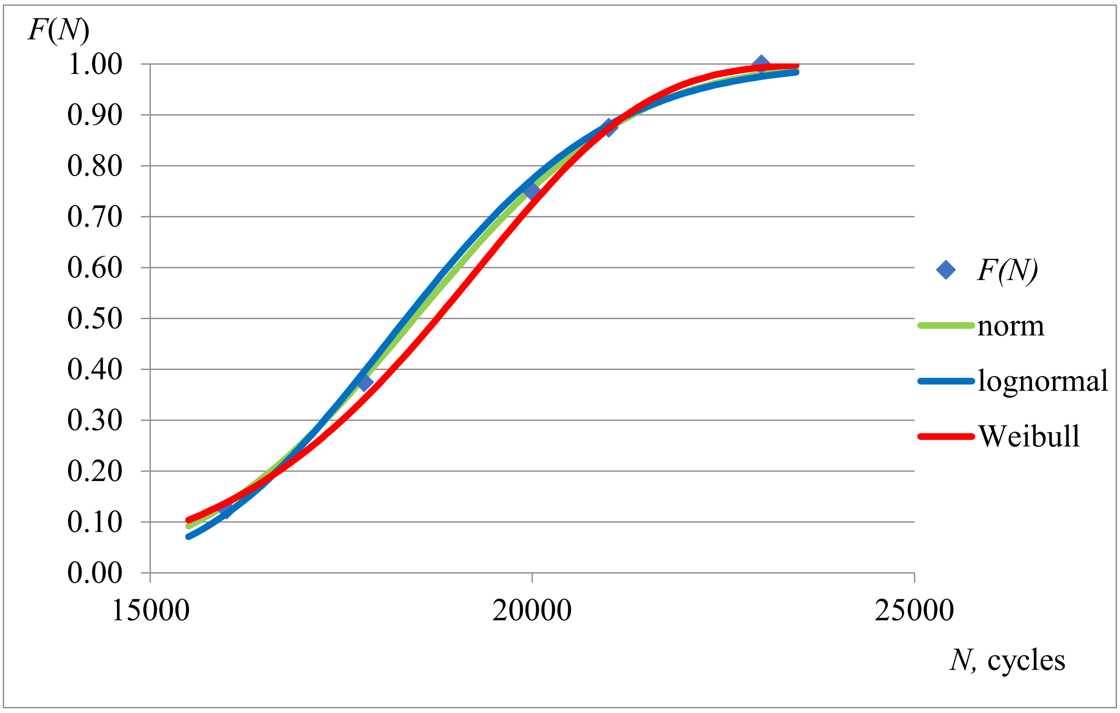

Fig. D.5. The cumulative probability function approximation for group 5-II, a = 7 mm.

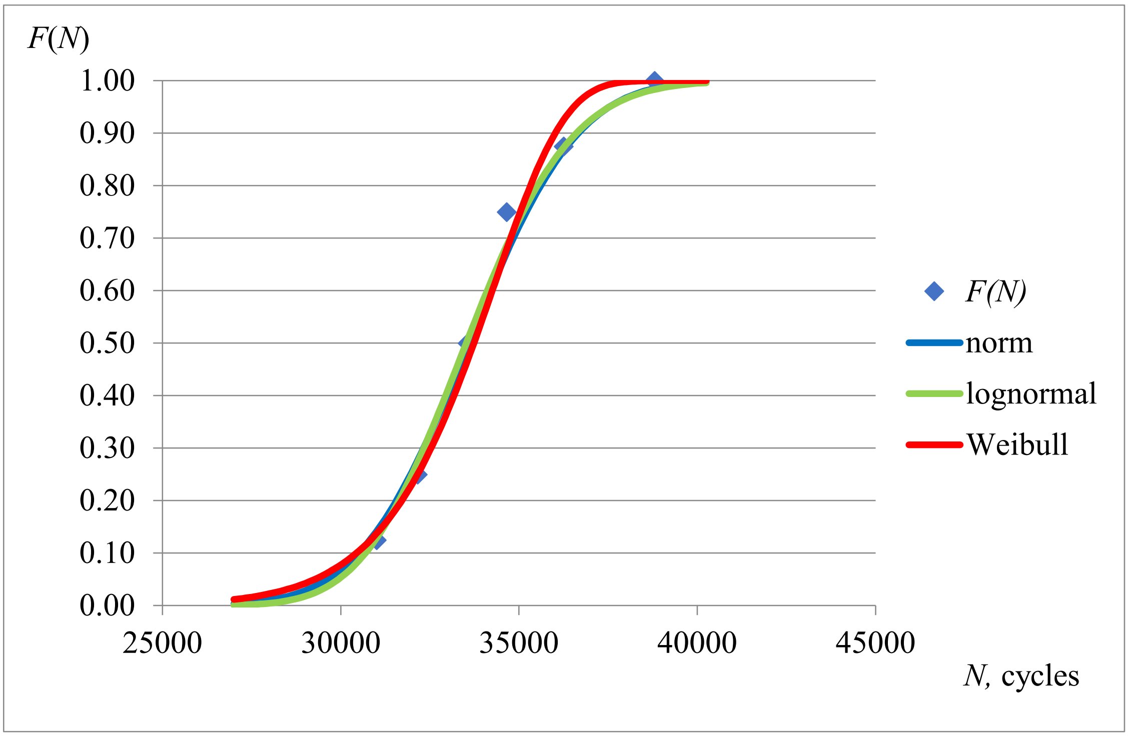

Fig. D.6. The cumulative probability function approximation for group 5-II, a = 10 mm.

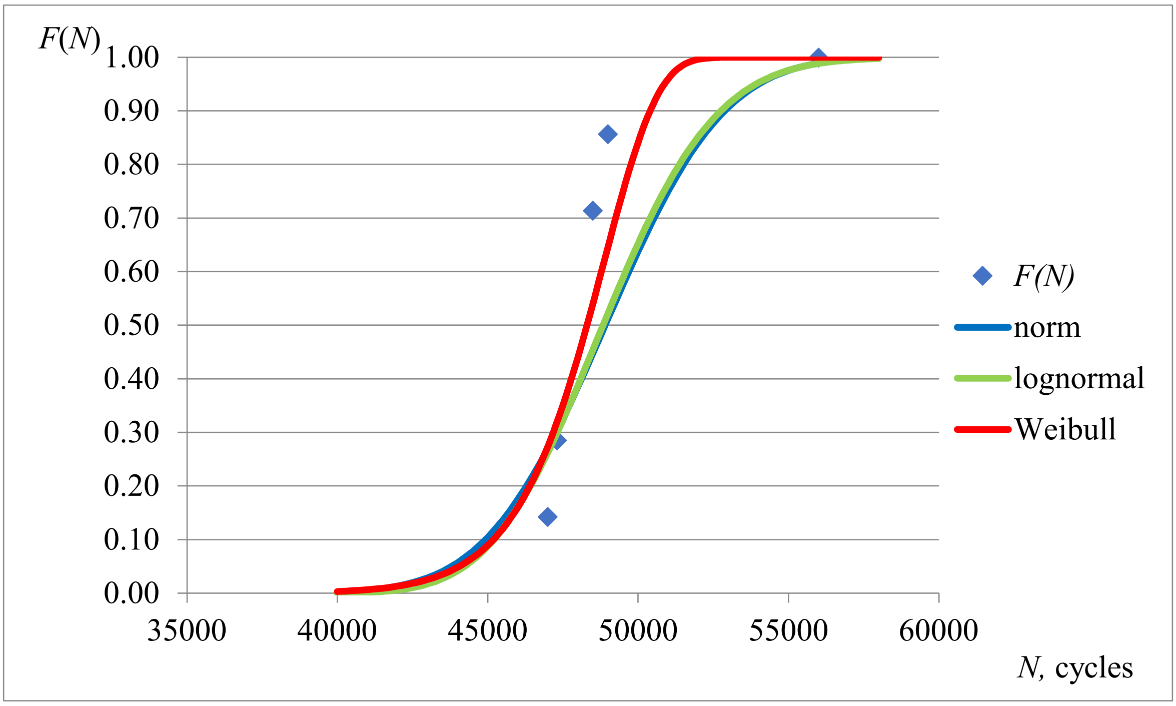

Fig. D.7. The cumulative probability function approximation for group 5-II, a = 15 mm.

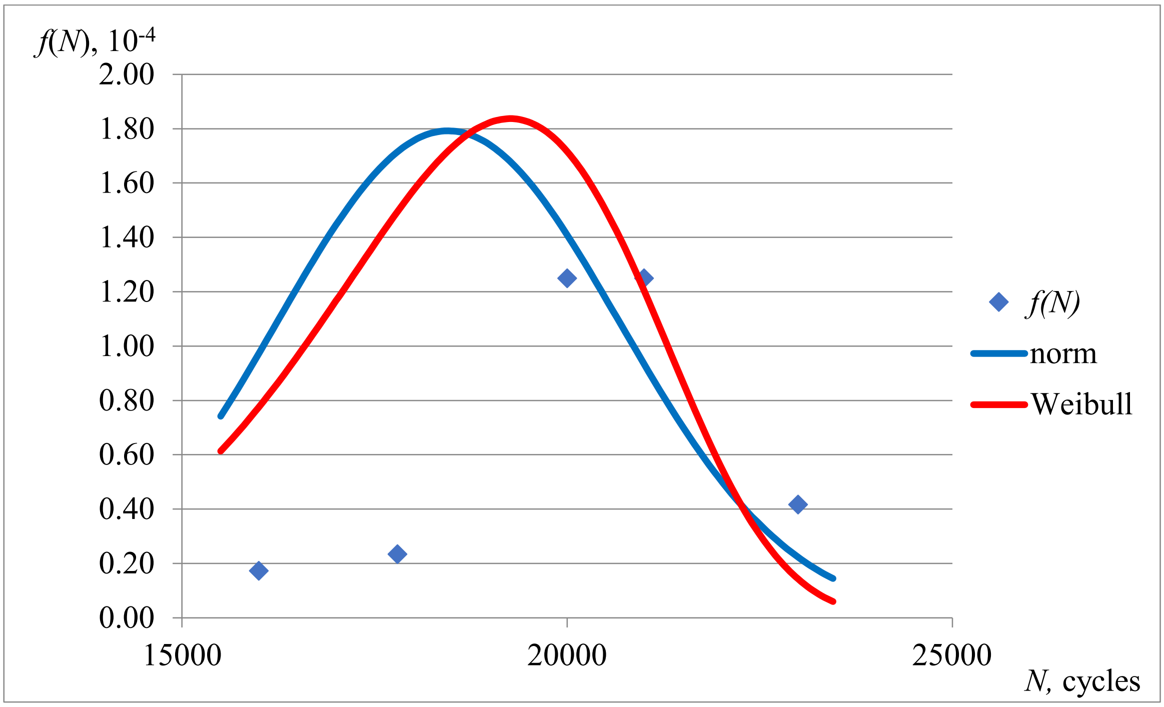

Fig. D.8. The probability density function approximation for group 5-II, a = 7 mm.

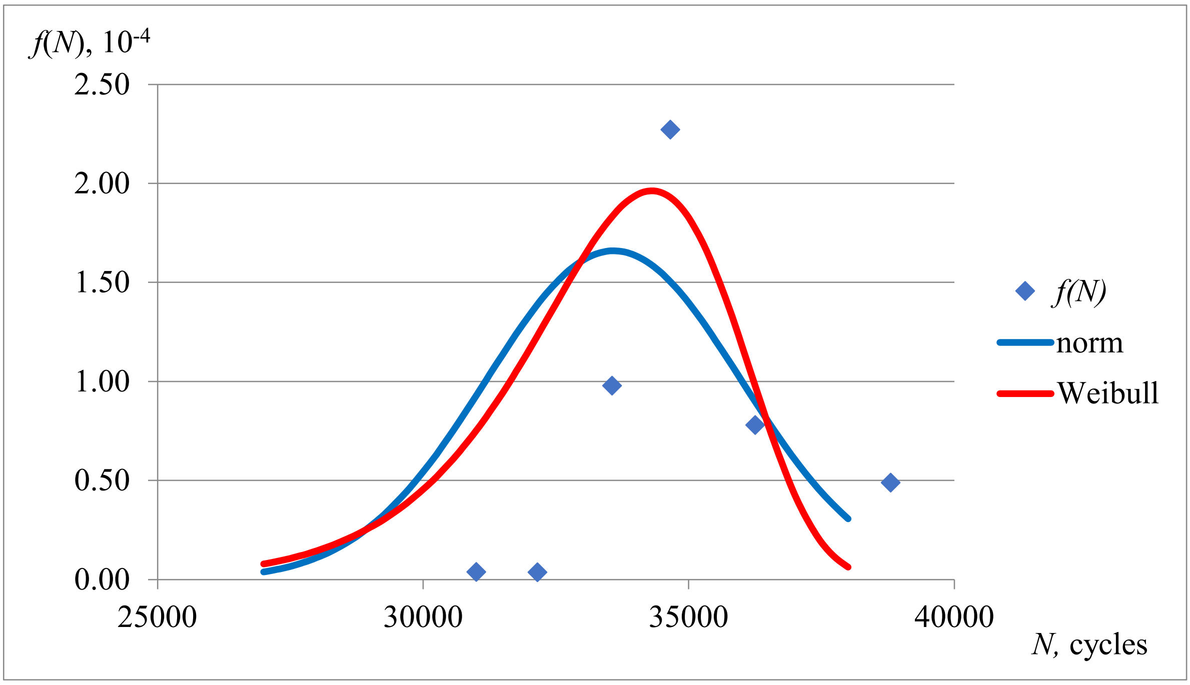

Fig. D.9. The probability density function approximation for group 5-II, *a* = 10 mm.

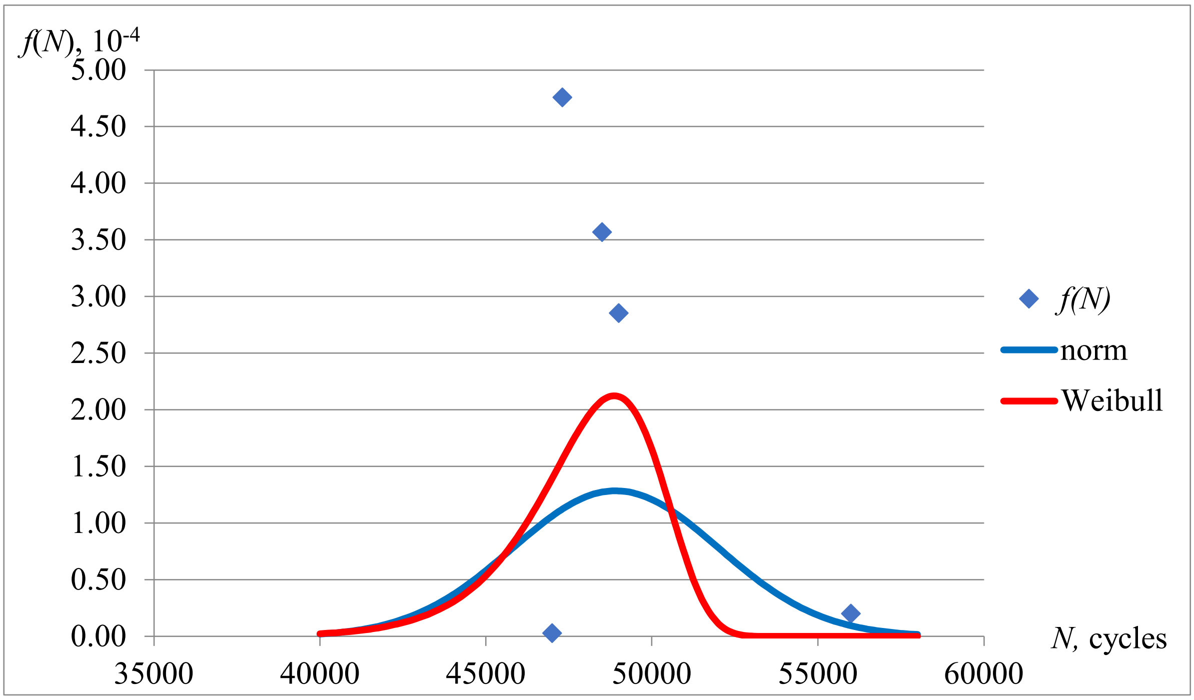

Fig. D.10. The probability density function approximation for group 5-II, *a* = 15 mm.

APPENDIX E. INTERGENERATIONAL COMPARISON GRAPHS FOR SET LENGTH

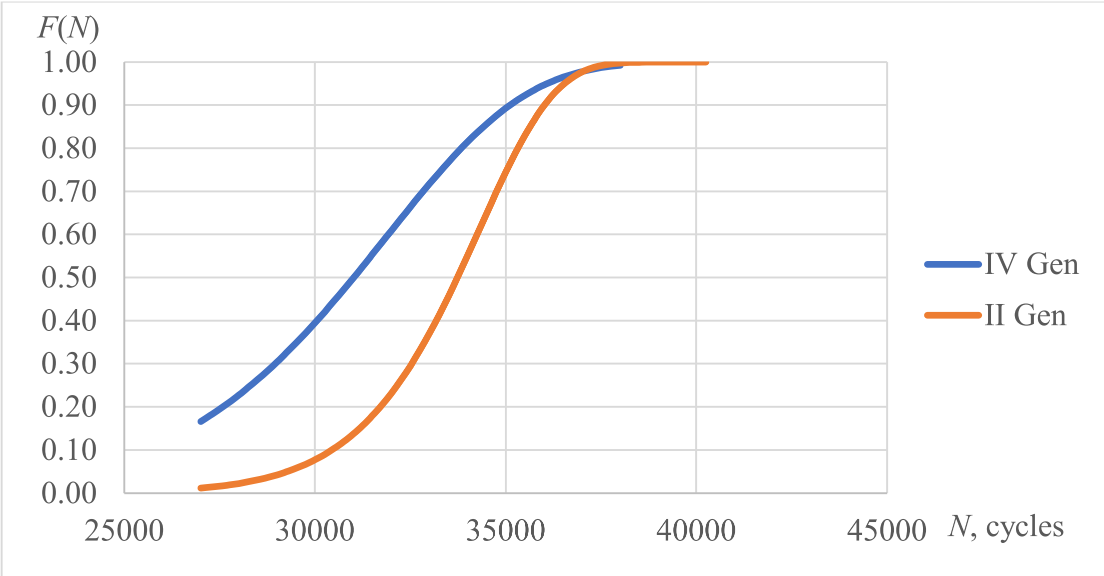

Fig. E.1. Weibull distribution for *a* = 10 mm comparison.

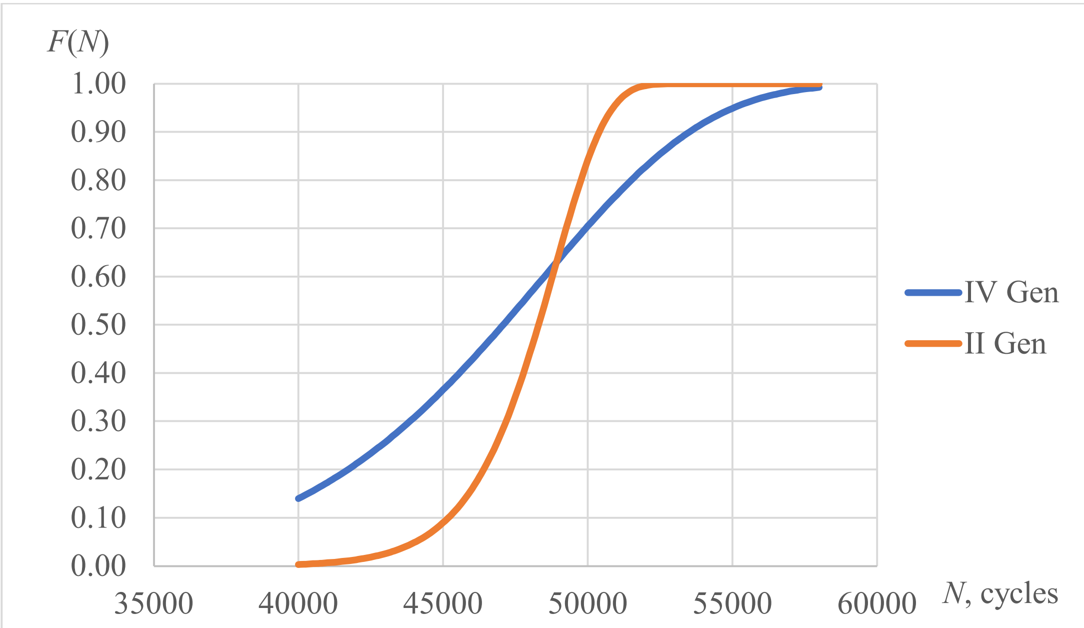

Fig. E.2. Weibull distribution for *a* = 15 mm comparison.

APPENDIX F. PROBABILISTIC GRAPHS FOR SET CYCLE NUMBERS

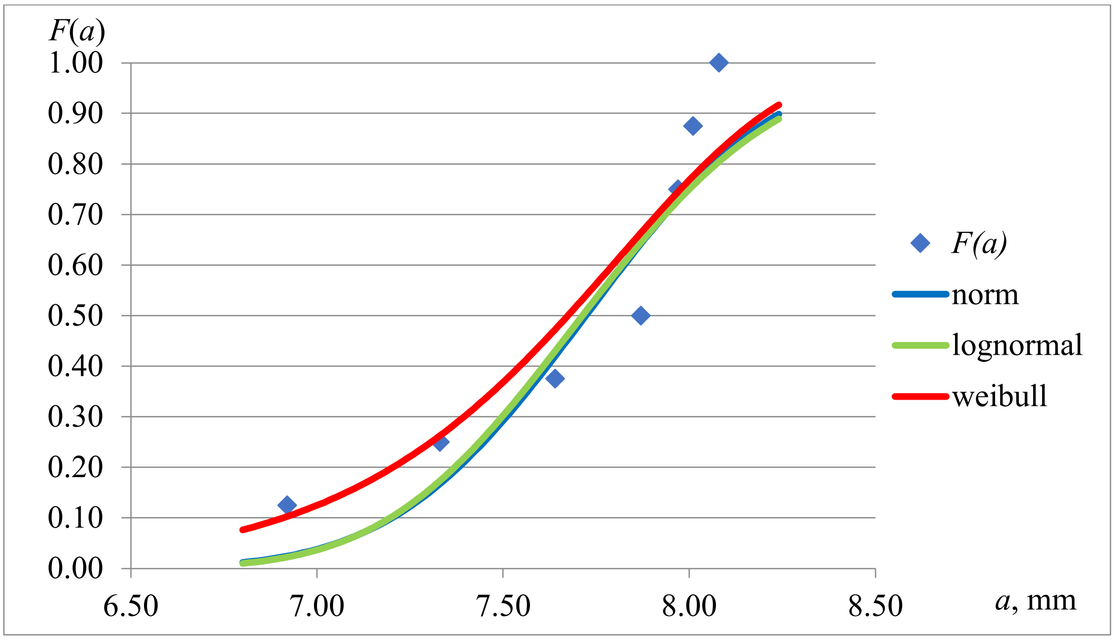

Fig. F.1. The cumulative probability function approximation for group 5-IV, $N = 20000$ cycles.

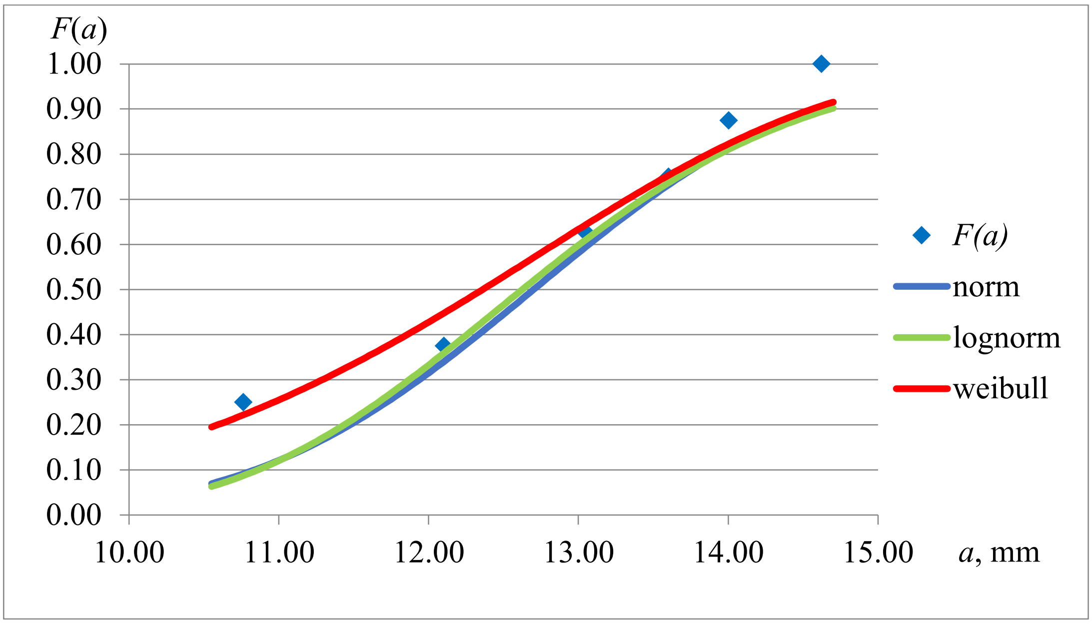

Fig. F.2. The cumulative probability function approximation for group 5-IV, $N = 40000$ cycles.

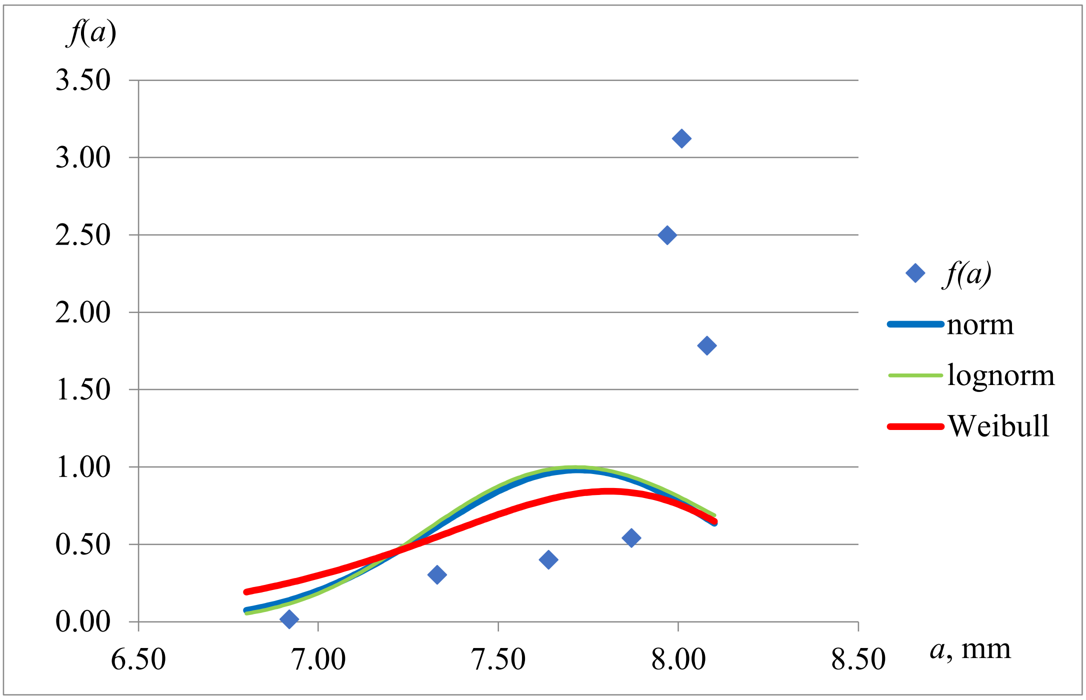

Fig. F.3. The probability density function approximation for group 5-IV, $N = 20000$ cycles.

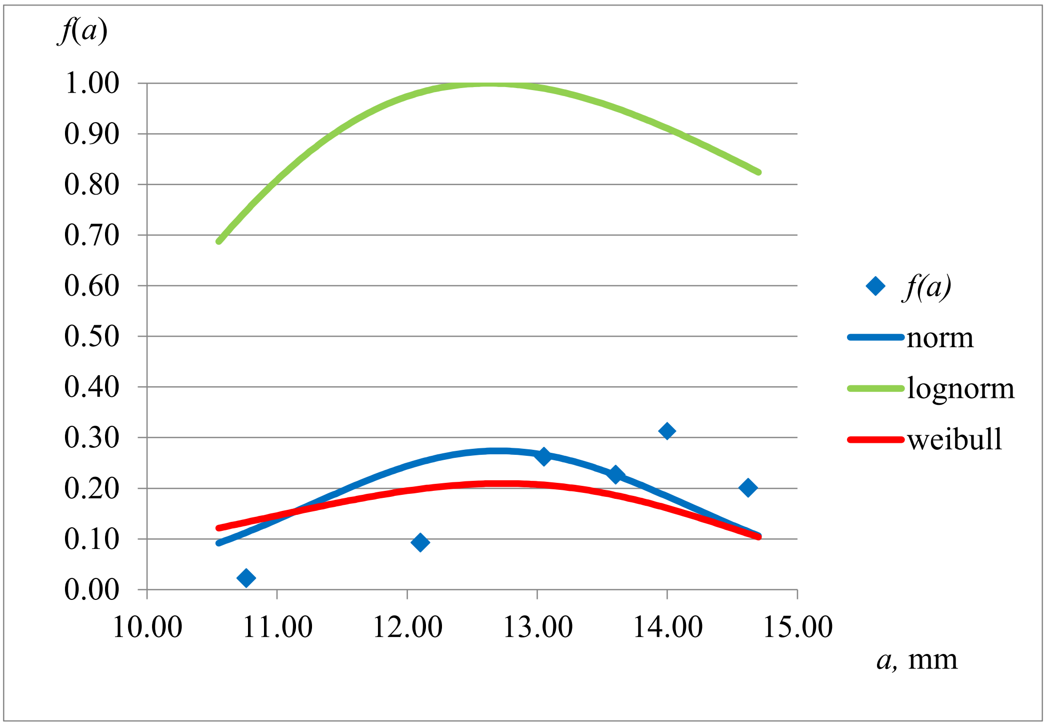

Figure F.4. The probability density function approximation for group 5-IV, $N = 40000$ cycles.

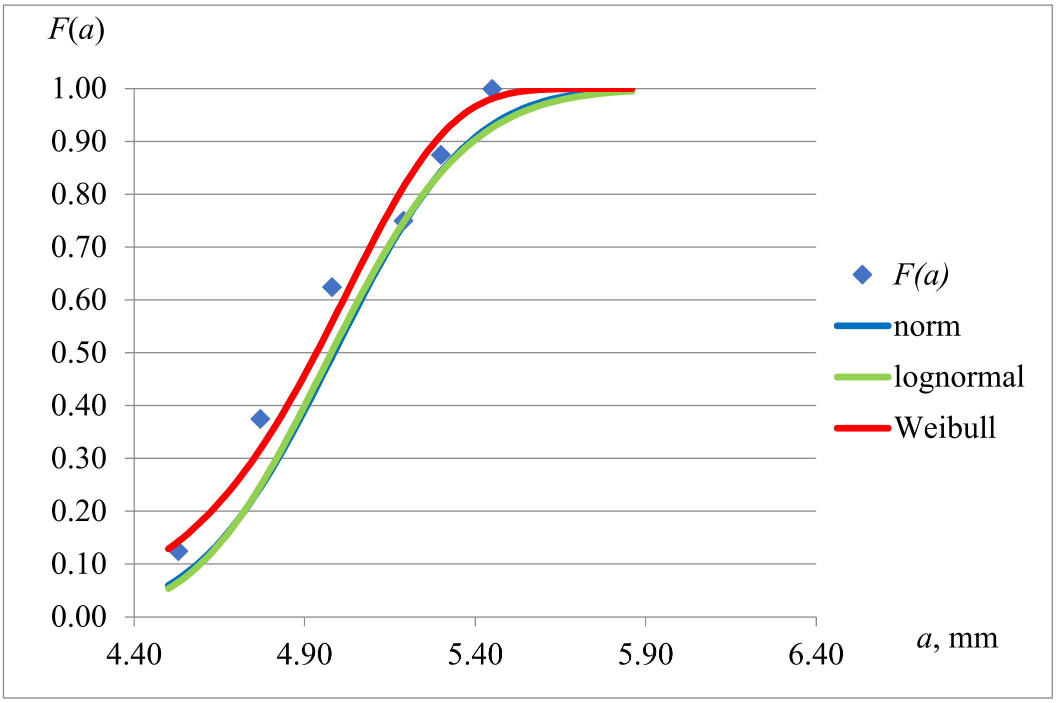

Fig. F.5. The cumulative probability function approximation for group 5-II, $N = 1000$ cycles.

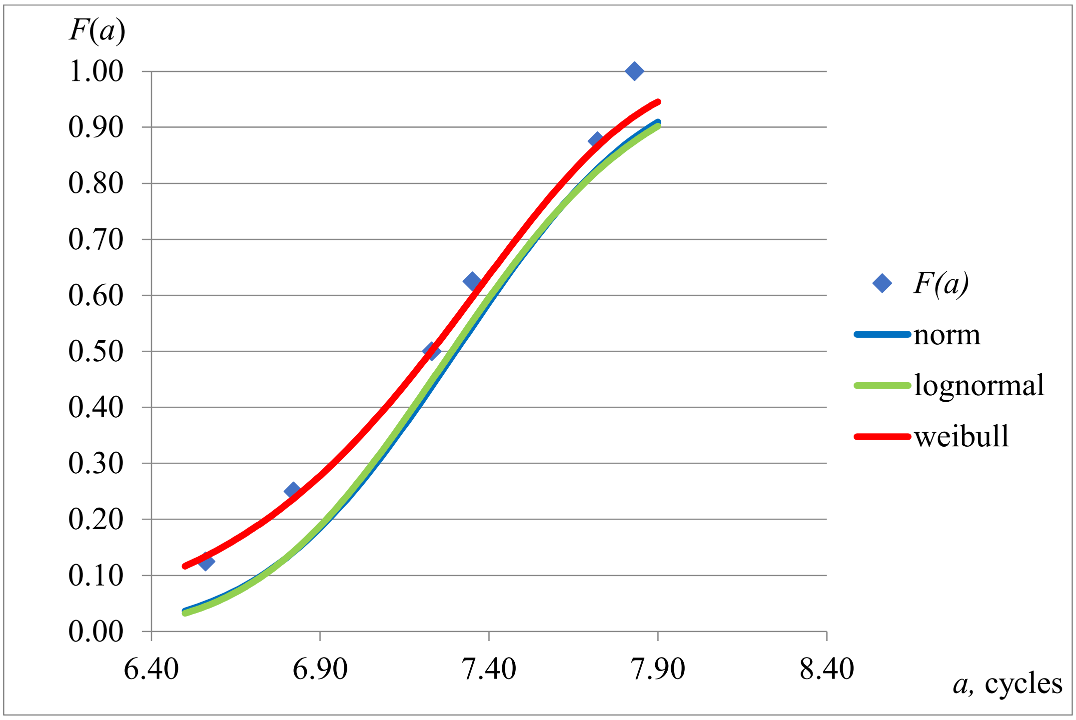

Fig. F.6. The cumulative probability function approximation for group 5-II, $N = 20000$ cycles.

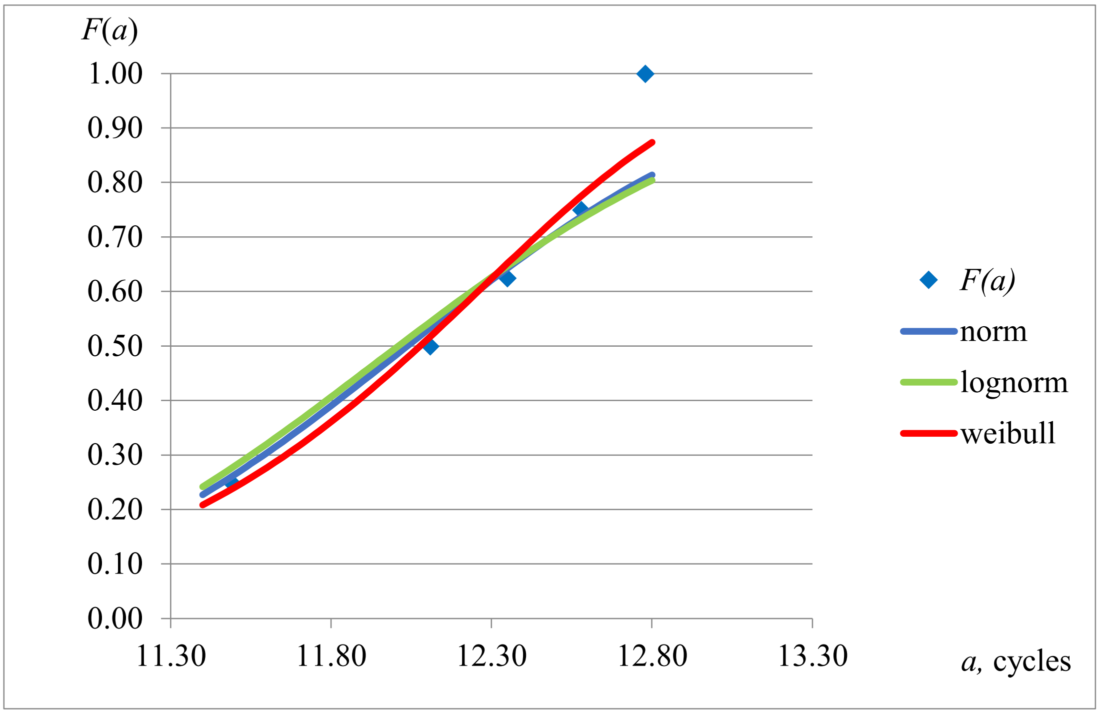

Fig. F.7. The cumulative probability function approximation for group 5-II, $N = 40000$ cycles.

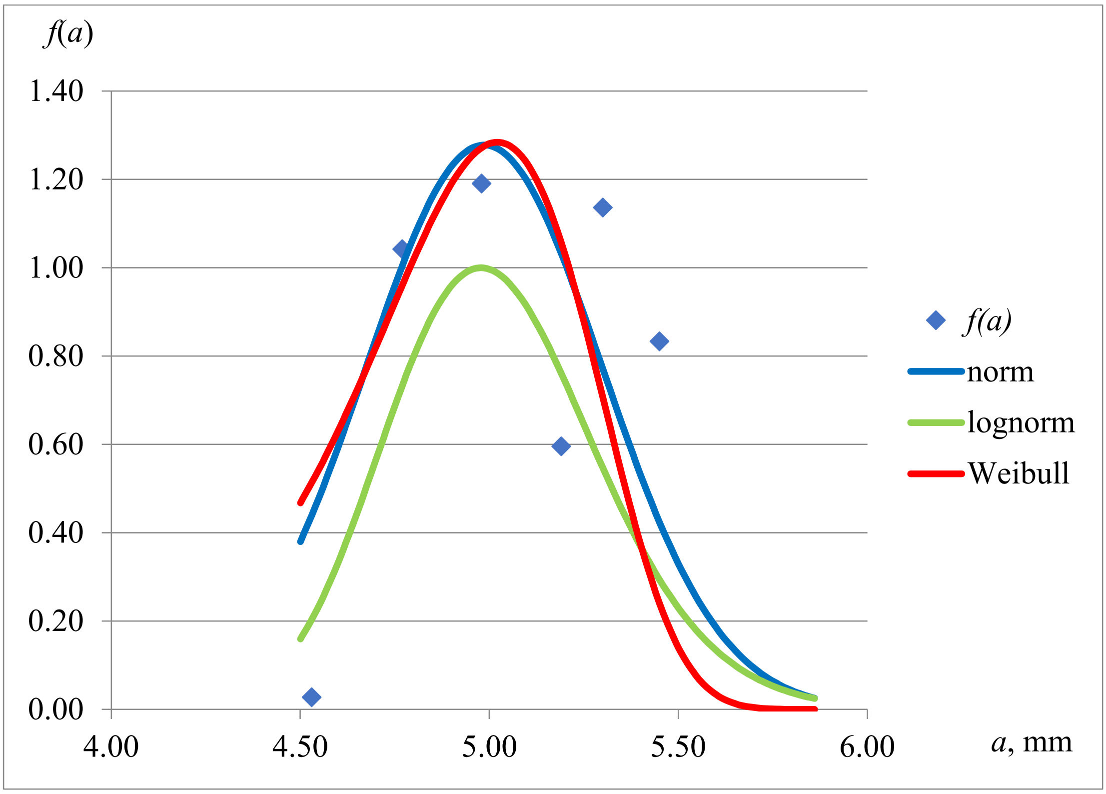

Fig. F.8. The probability density function approximation for group 5-II, $N = 1000$ cycles.

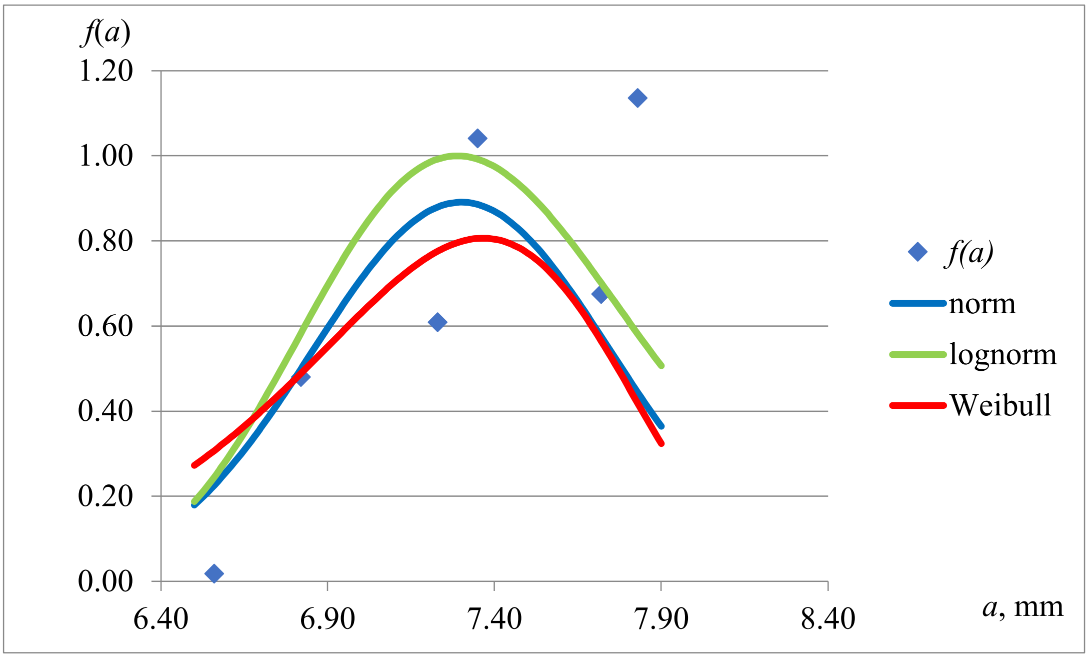

Fig. F.9. The probability density function approximation for group 5-II, $N = 20000$ cycles.

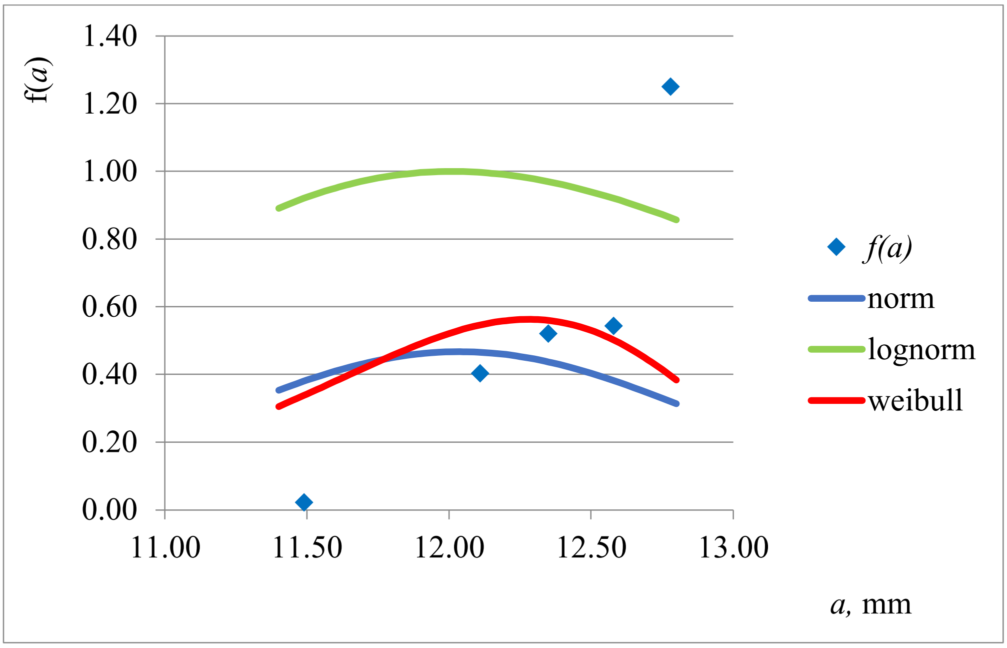

Fig. F.10. The probability density function approximation for group 5-II, $N = 40000$ cycles.

APPENDIX G. INTERGENERATIONAL COMPARISON GRAPHS FOR SET CYCLES NUMBER

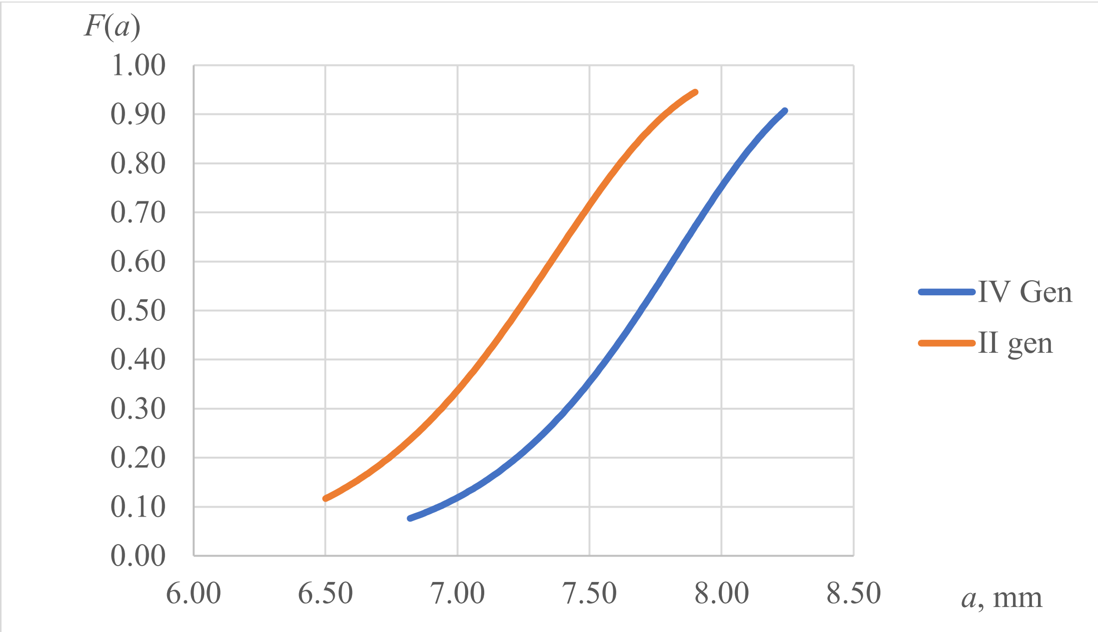

Fig. G.1. The probability of less than *a* mm crack appearance on $N = 20000$ cycles

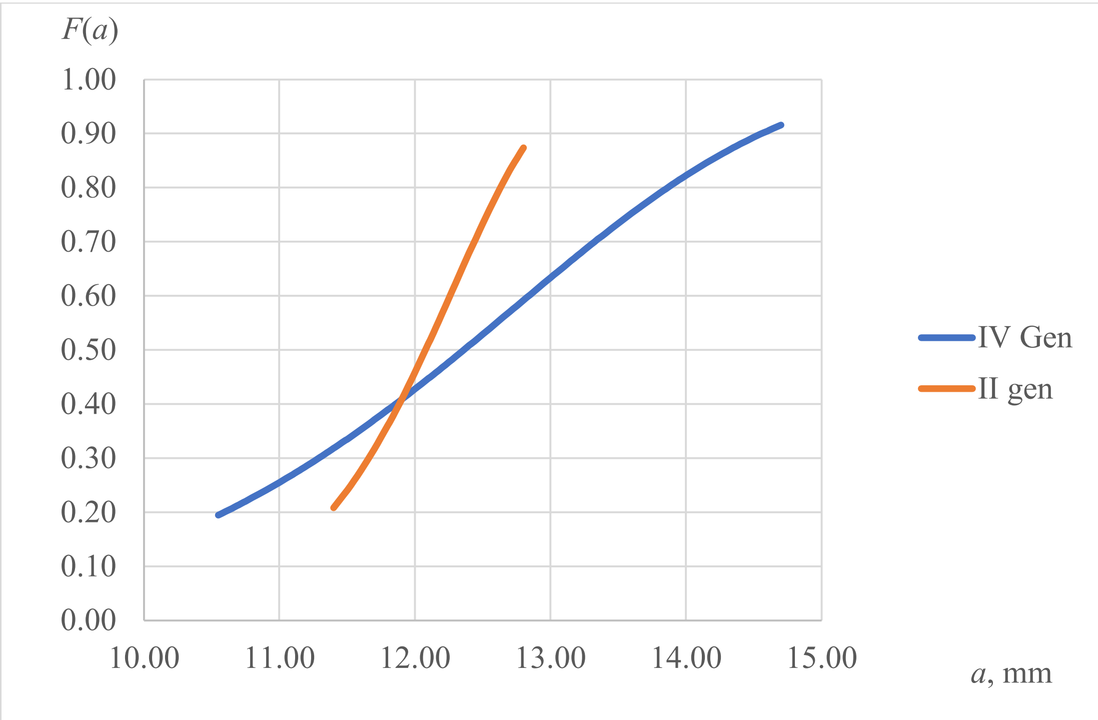

Fig. G.2. The probability of less than *a* mm crack appearance on $N = 40000$ cycles